Journal of Materials Chemistry A

ROYAL SOCIETY OF CHEMISTRY

REVIEW

View Article Online
View Journal | View Issue

Cite this: J. Mater. Chem. A, 2023, 11, 12659

Molecular designs, synthetic strategies, and properties for porphyrins as sensitizers in dye-sensitized solar cells

Yuzhe Zhang,[a] Tomohiro Higashino *[a] and Hiroshi Imahori *[ab]

Received 28th November 2022
Accepted 13th March 2023

DOI: 10.1039/d2ta09264f

rsc.li/materials-a

During the past decades, many efforts have been made to develop porphyrin sensitizers for dye-sensitized solar cells (DSSCs) due to their easy fabrication, low-cost production, and relatively high power conversion efficiency (PCE). Some of the molecular design principles and synthetic strategies have been proved to be able to construct high-performance porphyrin-based DSSCs. Herein, we focus on the promising and effective synthetic strategies for rationally designing porphyrins as sensitizers, and emphasize the crucial factors that have a profound impact on the photovoltaic performance to offer insightful views on the correlation between the molecular structure and photovoltaic performance.

10th anniversary statement

I would like to congratulate the *Journal of Materials Chemistry* on its 10th Anniversary. I previously served as a Deputy-Editor-in-Chief of the *Journal Materials Chemistry A* for four years and am still an Advisory Board member. At that time, the journal was steadily growing in terms of impact factor and submissions and I did not encounter any difficulties in the management. Throughout this activity, I have gotten to know many excellent researchers and RSC staff personally, and formed many relationships I still treasure. I hope the *Journal of Materials Chemistry* will continue to develop successfully long in to the future.

1. Introduction

Since the 19th century Industrial Revolution, fossil fuels have been the main resources in our daily life, which have driven the development of the world economy and the process of modernization. However, with the massive growth in the population of the world, the demand for fossil fuels keeps increasing, and will be inevitably be depleted in the future. Additionally, the excessive consumption of fossil fuels has led to a lot of serious environmental pollution and global warming in recent years. Thus, the impending energy crisis and environmental issues have become the key problems that need to be solved urgently in the world today. From these points of view, the development of sustainable and clean energy sources could be a reasonable solution. Solar energy, geothermal energy, wind energy, tidal energy, biomass energy, and nuclear energy possess their own advantages as alternative energy sources. Among these, the most abundant one is solar energy, which exceeds our global needs. Because solar energy is a substantially

[a]Department of Molecular Engineering, Graduate School of Engineering, Kyoto University, Nishikyo-ku, Kyoto, 615-8510, Japan. E-mail: t-higa@scl.kyotou.ac.jp; imahori@scl.kyotou.ac.jp

[b]Institute for Integrated Cell-Material Sciences (WPI-iCeMS), Kyoto University, Sakyo-ku, Kyoto, 606-8501, Japan

Yuzhe Zhang is a PhD student under the supervision of Prof. Hiroshi Imahori at Kyoto University. He received his Bachelor's (2017) and Master's (2020) degrees in applied chemistry from Tianjin University. His current research is focused on porphyrin dye-sensitized solar cells.

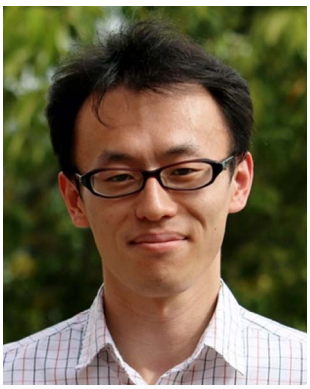

Tomohiro Higashino was born in 1986 in Osaka, Japan. He received his PhD in organic chemistry from Kyoto University in 2014. He was first an assistant professor (2013–2021) and then an associate professor (2021–present) in Prof. Imahori's group. His current interests include the development of novel π-conjugated materials and their applications.

infinite energy source, photovoltaics, which can directly convert solar energy to electricity, have attracted considerable attention. In particular, since the present style of dye-sensitized solar cells (DSSCs)[1] was reported by O'Regan and Grätzel[2] in 1991, they have been developed as an alternative to conventional silicon-based solar cells in these past decades because of their ease of fabrication, low-cost production, high power conversion efficiency (PCE), and advantages in indoor lighting.

A schematic illustration of the components and operational principles of DSSCs is illustrated in Fig. 1. The typical device of DSSCs is based on a sandwich structure, which consists of the following components: a transparent conductive oxide (TCO) electrode, mesoporous TiO_2, sensitizer (S), electrolyte solution, counter Pt electrode, and TCO. The photocurrent is generated by the following processes: (1) a sensitizer attached to TiO_2 is excited from the ground state (S) to an excited state (S*) by harvesting sunlight; (2) the photoexcited sensitizer injects an electron into a conduction band (CB) of TiO_2, whereby the oxidized sensitizer ($S^{\bullet+}$) is generated; (3) the resultant oxidized sensitizer ($S^{\bullet+}$) is reduced by redox shuttles in the electrolyte solution (Red: Co^{2+}, Cu^{1+} complex, or I^- species); (4) the electron in the CB is transferred to the counter electrode through an external circuit; (5) the oxidized redox shuttles (Ox: Co^{3+}, Cu^{2+} complex, or I_3^- species) are reduced to regenerate the corresponding species at the surface of the counter electrode, and the circuit is thus completed.

Sensitizers (or dyes) play an important role in the photocurrent generation and device performance of DSSCs. In the early stage of DSSCs, ruthenium-based complexes, such as **N3** (ref. 3) and **N719** (ref. 4) (Fig. 2), were applied to DSSCs and achieved excellent PCEs of up to 11% as a result of their excellent light-harvesting property, long excited-state lifetime, and high photostability. Furthermore, a lot of efforts have been directed towards the ligands for further optimization: for instance, work on the black dye **N749** (ref. 5), whose broad absorption covers the entire visible spectrum, for extending it into the near-infrared (NIR) region (~920 nm); the amphiphilic sensitizer **Z907** (ref. 6), for exhibiting long-term thermostability with a polymer gel electrolyte; the heteroleptic ruthenium sensitizer **CYC-B11** (ref. 7) with a hexylthio-bithiophene moiety in ancillary ligands, which possesses an excellent light-harvesting capacity (Fig. 2). However, the high price and limited supply of the ruthenium metal are problematic for its large-scale use in the industrial production of DSSCs. Therefore, ruthenium-free dyes, such as metal-free or cheap metal–organic dyes, have been explored towards high-performance DSSCs because their optical and electronic properties can be easily tuned by molecular modifications. To date, many metal-free organic dyes based on the donor–π-bridge–acceptor (D–π–A) structure have been developed and have attained excellent PCEs owing to their improved light-harvesting abilities by intramolecular charge transfer (ICT) from the donor to acceptor moieties (*i.e.* push–pull structures).[8] The representative examples include **C272** (ref. 9), **SGT-130** (ref. 10), and **MK-2** (ref. 11) (Fig. 2), which are comparable with traditional ruthenium-based complexes. In addition, D–π–A dyes provide wide possibilities for further modification on the donor, π-bridge, and acceptor moieties to achieve higher PCEs. For instance, **C281** (ref. 12), **SGT137** (ref. 13), and **ADEKA-1** (ref. 14) (Fig. 2) have given PCEs of more than 12%.

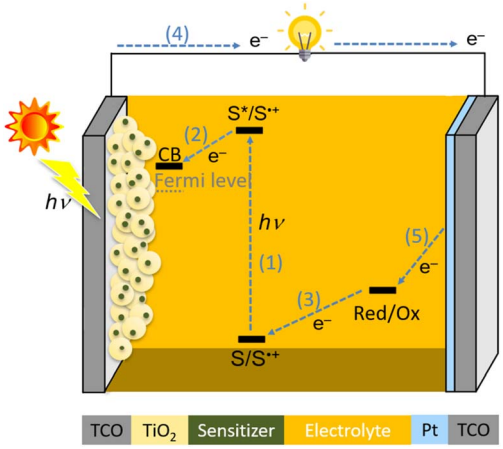

Fig. 1 Schematic illustration of the components and operational principles of a DSSC.

Porphyrin, an aromatic macrocycle with an 18π-electron system, has an intense Soret band (400–500 nm) and moderate Q-bands (500–600 nm) in the visible region, as well as extremely high molar absorption coefficients (ε ~10^4–10^5 M^{-1} cm^{-1}), surpassing other conventional dyes. Moreover, the introduction of substituents at the four *meso*- and eight β-positions of the porphyrin can easily tune the electronic, optical, electrochemical, and photophysical properties (Fig. 3). Additionally, porphyrins and related macrocycles are widely found in natural plants as important components for converting sunlight into chemical energy efficiently. Inspired by this elegant solar-energy-conversion process, researchers have attempted to utilize porphyrins as potential sensitizers for DSSCs. However, since the first application of porphyrins to DSSCs by Kay and Grätzel[15] in 1993, work on porphyrin-based DSSCs stagnated (PCE < 7.1%) in the decades from 1990 to 2009 because of their weak light-harvesting abilities around 500 nm and over 600 nm. To overcome the bottleneck and kick start the work again in this field, porphyrin sensitizers have adopted a D–π–A structure, as seen in metal-free organic dyes. In 2010, Yeh *et al.* reported **YD2** (ref. 16) (Fig. 4), bearing

Hiroshi Imahori received his Doctor of Science from Kyoto University in 1990. After post-doctoral training at the Salk Institute for Biological Studies, he was first an assistant and then associate professor at Osaka University. Since 2002, he has been a full professor at Kyoto University. His current interests involve solar energy conversion and organic functional materials.

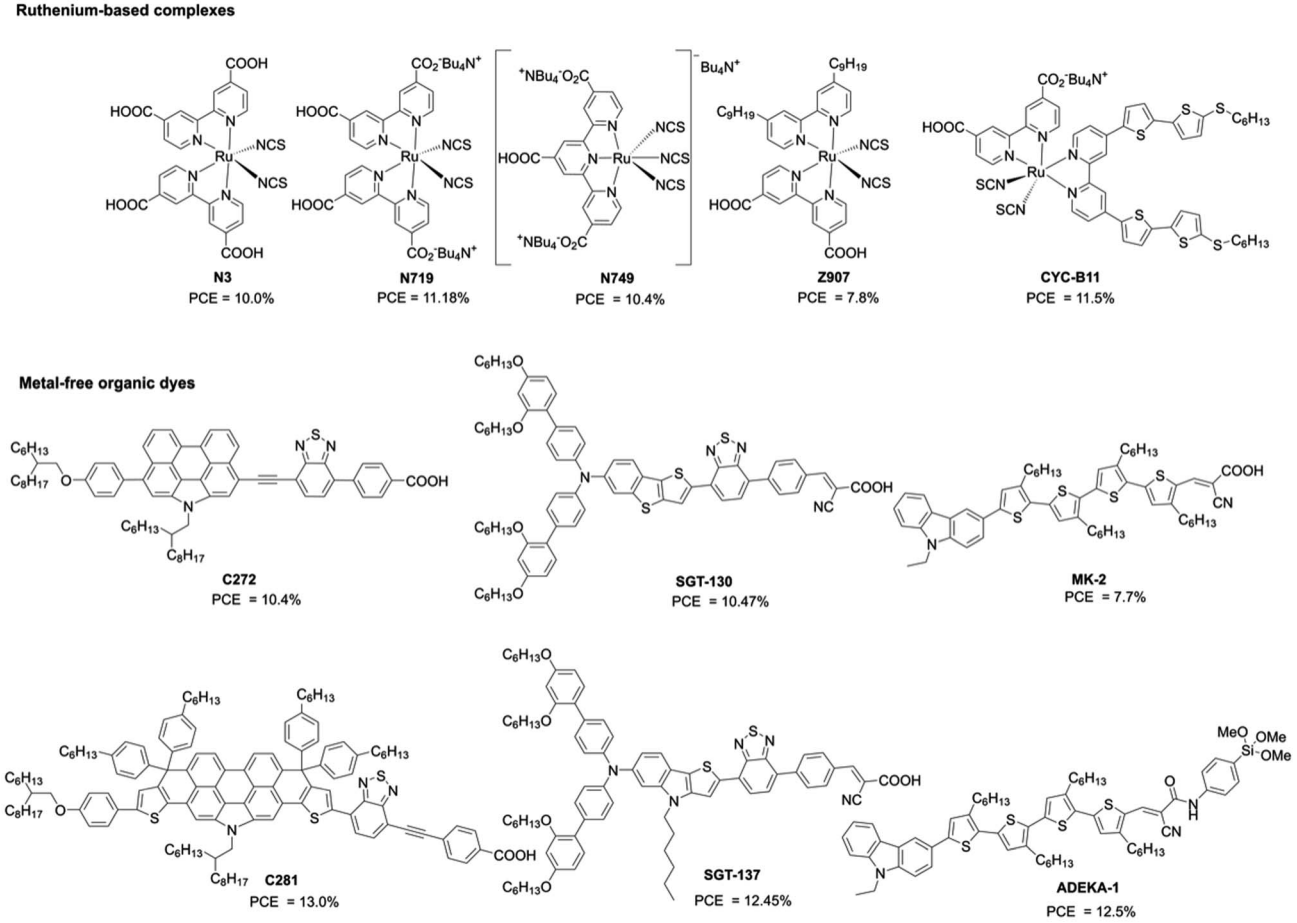

Fig. 2 . Chemical structures of some representative dyes for DSSCs.

a bis(4-hexylphenyl)amine donor moiety and a 4-ethynylbenzoic acid acceptor moiety, obtaining a PCE of 11% with the I^-/I_3^- redox couple. Although the I^-/I_3^- redox couple is the most commonly used redox mediator, the open circuit voltage (V_{OC}) value of DSSCs with the I^-/I_3^- redox couple is limited to 0.7–0.8 V due to the large overpotential needed for dye regeneration.[1] To surmount this V_{OC} limitation, $Co^{II/III}$ trisbipyridyl ($[Co(bpy)_3]^{2+/3+}$) has been applied as a second-generation redox couple,[1] since DSSCs with the $[Co(bpy)_3]^{2+/3+}$ redox shuttle were found to exhibit a high V_{OC} value of up to 1.0 V owing to its more positive redox potential. It is noteworthy that the use of bulky substituents on dyes is essential to suppress the undesirable charge recombination (CR). Indeed, alkoxy-wrapped porphyrin dyes have been designed for DSSCs with the $[Co(bpy)_3]^{2+/3+}$ redox couple, and in this regard, the **YD2** analogue **YD2-*o*-C8** (ref. 17) (Fig. 4) showed a PCE of 11.9% with the $[Co(bpy)_3]^{2+/3+}$ redox couple (*vide infra*).

Further optimizations of the D–π–A structure led to the dyes **SM315**,[18] **GY50** (ref. 19) (Fig. 4), and **SGT-021** (ref. 20) (Fig. 4), which achieved impressive PCEs of up to *ca.* 13%. Although the PCEs of porphyrin-based DSSCs have increased gradually,[21–27] there is still plenty of room for boosting the device performance by the rational molecular design of porphyrin sensitizers. Therefore, in this review article, we highlight the rational molecular designs, versatile synthetic strategies, and desired properties of high-performance porphyrin dyes in DSSCs. The representative photovoltaic parameters of porphyrin-based DSSCs are summarized in Tables 1 and 2.

2. D–π–A-structured porphyrins

2.1 *Meso*-functionalized porphyrins

Adoption of a push–pull structure by donors and acceptors, respectively, is the most effective strategy in terms of the molecular design of high-performance porphyrin dyes because of their enhanced light-harvesting abilities and electron-injection efficiencies (ϕ_{inj}) based on ICT. Generally, push–pull porphyrins consist of a donor, π-porphyrin core, and acceptor. Because *meso*-substituted porphyrins can be relatively easily synthesized and *meso*-substituents can effectively affect their electronic structures, well-designed *meso*-substituted push–pull porphyrins have been extensively studied for application in DSSCs. Among them, *trans*-A_2BC-type push–pull porphyrin dyes are representative examples. The common synthetic protocols are shown in Scheme 1. Route a, which was reported by Yeh *et al.* for the synthesis of **YD2** (Fig. 4),[28] is the most frequently adopted strategy. Here, the *meso*-(triisopropylsilyl)ethynyl porphyrin **1** undergoes bromination to give **2**, which takes part

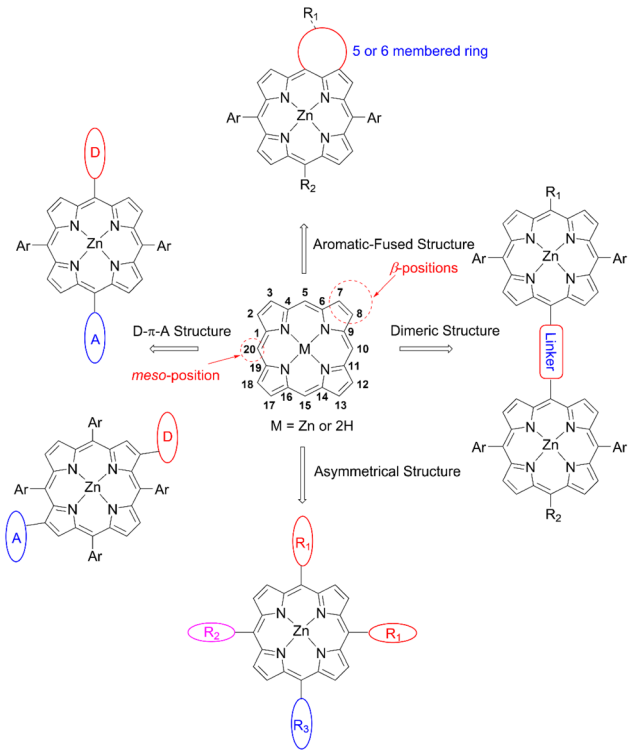

Fig. 3 Structure and numbering of the porphyrin molecule, and common design principles of porphyrins for DSSCs.

in a subsequent Buchwald–Hartwig amination or Suzuki–Miyaura coupling reaction to introduce a donor moiety, such as diarylamino and indoline groups. Then, the triisopropylsilyl (TIPS) group of **3** is deprotected using tetrabutylammonium fluoride (TBAF), and then undergoes a Sonogashira coupling reaction to afford the *trans*-A_2BC-type push–pull porphyrin dye **4**. According to this strategy, benchmark push–pull porphyrin dyes, for example, **YD2-*o*-C8**, **GY50**, and **SM315** (Fig. 4), have been synthesized. One of the advantages of this protocol is that we can easily change the donor and/or acceptor moieties to evaluate the effect of different molecular structures. Actually, the incorporation of additional electron-withdrawing benzothiadiazole (BTD) between the ethynyl and benzoic acid groups in **GY50** and **SM315** is an effective way to obtain high-performance sensitizers.

In 2017, Kim and co-workers[20] designed and synthesized two porphyrin sensitizers, namely **SGT-020** and **SGT-021** (Fig. 4), according to this route a, and studied the effects of the electron-donating ability and bulkiness on the photovoltaic performance with **SM315** as a reference. Among the three dyes, **SGT-021** with the rigid and electron-rich fluorenyl moieties exhibited the highest PCE of 12.0% because of the improved short circuit current density (J_{SC}) and V_{OC} values. The electron-rich nature of fluorenyl moieties enhanced the light-harvesting ability due to the red-shifted absorption. In addition, the rigid fluorenyl moieties can ensure an efficient blocking effect and suppress undesirable CR. Wang and co-workers[29] screened D–π–A-type porphyrin dyes with various donor moieties by using

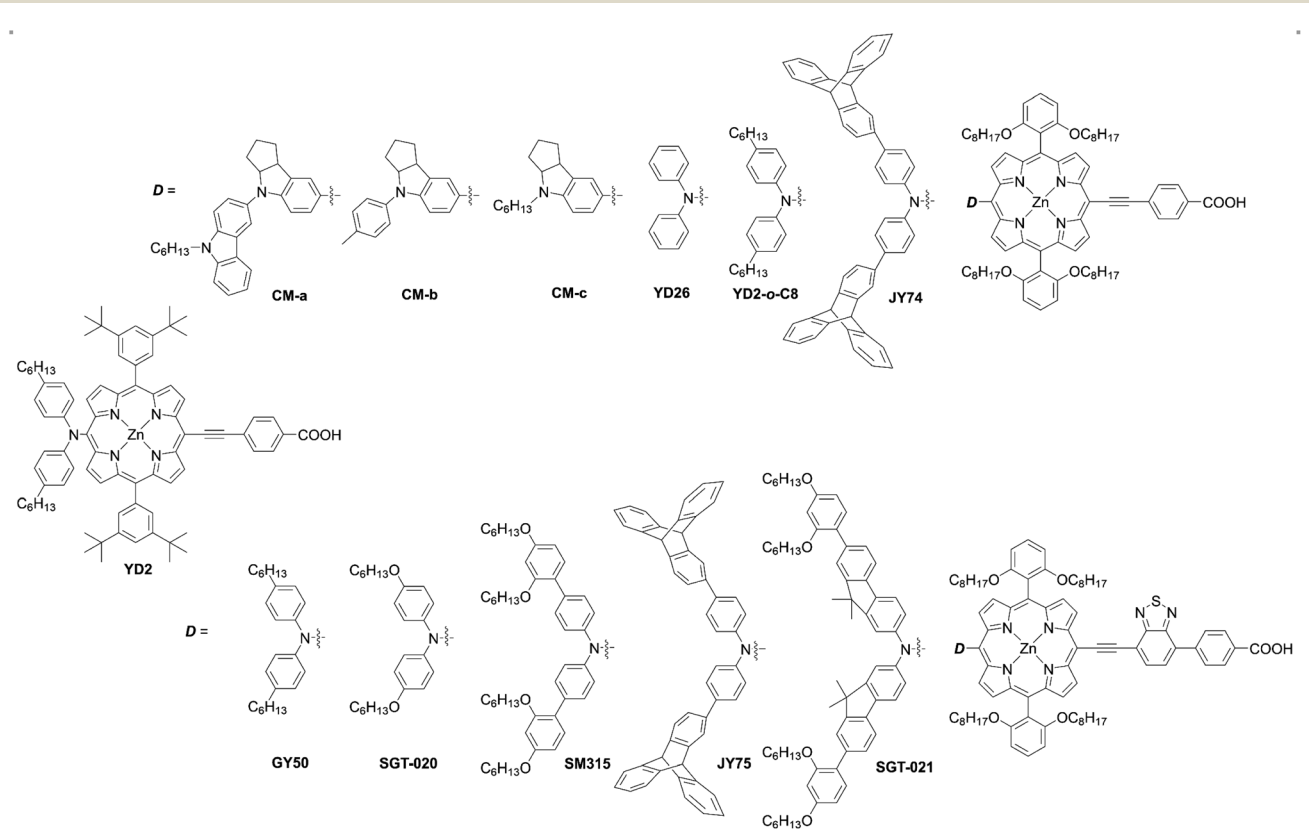

Fig. 4 Chemical structures of representative *meso*-functionalized D–π–A type porphyrins.

Table 1 Photovoltaic parameters of porphyrin-based DSSCs with I^-/I_3^- as the redox shuttle, under simulated AM 1.5 G full sun illumination (input power was 100 mW cm^{-2} without additional illumination)

Dye	J_{SC} (mA cm^{-2})	V_{OC} (V)	F. F. (fill factor)	PCE (%)	Ref.
YD2	18.6	0.77	0.764	11	16
CM-a	19.56	0.668	0.651	8.5	29
CM-b	22.58	0.734	0.645	10.7	29
CM-c	20.88	0.726	0.641	9.7	29
YD2-*o*-C8	18.81	0.701	0.646	8.5	29
YD2-*o*-C8T	15.6	0.73	0.68	7.7	30
YD2-*o*-C8	17.3	0.78	0.65	8.8	30
ZnPSi2[a]	9.60	0.698	0.702	4.7[b]	32
YD2-*o*-C8	15.0	0.754	0.684	7.7[b]	32
YD26	12.92	0.662	0.62	5.3[f]	38
JY74	14.58	0.681	0.63	6.3[f]	38
JY75	16.50	0.673	0.61	6.8[f]	38
XW29	21.26	0.716	0.666	10.14	45
XW30	19.67	0.678	0.651	8.68	45
XW31	22.06	0.720	0.658	10.46	45
XW32	20.13	0.677	0.647	8.82	45
XW17[a]	15.96	0.700	0.729	8.14	50
ZnPNTz[a]	7.33	0.648	0.765	3.63	50
ZnPBA[a]	16.26	0.713	0.719	8.3[b]	51
ZnPBAT[a]	19.33	0.719	0.724	10.1[b]	51
YD2[a]	17.05	0.742	0.718	9.1[b]	51
ZnPBAT-*o*-C8	18.6	0.737	0.665	9.1[b]	52
ZnPBAT-*o*-C8C4[a]	15.9	0.673	0.684	7.3[b]	52
ZnPBAT-*o*-C8C8[a]	14.1	0.706	0.709	7.0[b]	52
YD2-*o*-C8[a]	16.4	0.777	0.676	8.6[b]	52
21	11.6	0.563	0.62	4.1	53
22	14.0	0.586	0.58	4.7	53
23	8.9	0.528	0.65	3.1	53
24	12.9	0.598	0.60	4.6	53
25	10.5	0.586	0.65	4.0	53
26	11.1	0.600	0.59	3.9	53
27	13.3	0.519	0.61	4.2	53
28	11.7	0.482	0.53	3.0	53
SK7	13.25	0.663	0.745	6.54	54
YD2	15.42	0.694	0.727	7.78	54
SK7	0.739	0.584	0.778	19.7[c]	54
YD2	0.721	0.602	0.783	20.0[c]	54
ZnBD1[a]	13.9	0.67	0.64	5.9[f]	56
ZnBD2[a]	18.4	0.71	0.57	7.5[f]	56
fused-Zn-1	10.6	0.62	0.62	4.1	59
Zn-1	6.7	0.61	0.68	2.8	59
ZnQMA	11.2	0.72	0.68	5.2	61
ZnQDA	9.3	0.67	0.64	4.0	61
ZnPQI[a]	13.9	0.68	0.71	6.8	62
ZnQMA[a]	13.2	0.71	0.67	6.3	62
fused-ZnP	0.88	0.51	0.67	0.3	63
YH6	16.12	0.58	0.72	6.7[f]	65
YH7	15.12	0.57	0.66	5.7[f]	65
YH8[a]	12.51	0.60	0.72	5.3	66
YH9[a]	16.16	0.63	0.68	6.9	66
YH10[a]	17.16	0.63	0.70	7.5	66
AfZnP[a]	11.1	0.678	0.723	5.47	68
DfZnP[a]	15.4	0.669	0.708	7.31	68
GY50	16.3	0.732	0.713	8.53	68
LD14	18.2	0.716	0.704	9.2	71
LDD1	18.8	0.692	0.677	8.8	71
LDD1+LD14	21.3	0.705	0.692	10.4	71
ZnPTD[a]	14.7	0.595	0.712	6.22	72
LDD1[a]	19.0	0.633	0.680	8.17	72
JY06	11.18	0.63	0.61	4.3[f]	73
JY07	13.20	0.65	0.62	5.3[f]	73
75	8.55	0.610	0.6996	3.65	80
76	7.21	0.600	0.6741	2.92	80
77	4.35	0.590	0.7206	1.85	80
78	8.37	0.600	0.7138	3.60	80
BC2H[a]	5.95	0.60	0.75	2.7[b]	81
YD2[a]	17.6	0.72	0.70	8.9[b]	81
LS-01	12.58	0.53	0.70	4.7[f]	82
LS-11	16.13	0.52	0.64	5.4[f]	82
H2PE1	5.26	0.54	0.73	2.1[f]	82
LS-17	14.90	0.54	0.64	5.1[f]	84
LS-43	14.67	0.52	0.61	4.6[f]	84
LS-45	17.43	0.54	0.64	6.0[f]	84
XW10	17.90	0.711	0.684	8.60	42
XW40	18.67	0.730	0.683	9.31	85
XW41	16.77	0.695	0.701	8.16	85
XW40[a,d]	19.59	0.748	0.719	10.5[f]	85
XW41[a,d]	19.63	0.726	0.715	10.2[f]	85
XW60	16.77	0.715	0.731	8.8	87
XW61	20.75	0.763	0.739	11.7	87
XW62	20.70	0.762	0.732	11.6	87
XW63	20.63	0.763	0.737	11.6	87
XW61[a]	21.41	0.775	0.747	12.4	87
XW51	20.07	0.781	0.702	11.1	88
XW51[e]	18.05	0.720	0.708	9.2	87
XW51[a,e]	20.13	0.738	0.705	10.5	87

[a] Coadsorbed with **CDCA**. [b] Obtained after ageing for several days. [c] Measured under 6000 lx intensity from a T5 fluorescent tube (input power was 1.70 mW cm^{-2}). [d] Co-sensitized with **Z1** (Fig. 19). [e] Co-sensitized with **Z2** (Fig. 18). [f] Corrected on the basis of significant figures.

theoretical calculations and found that the indoline motifs may be suitable donor groups because of their nonplanar geometry and the large oscillator strength of the S_0–S_1 transition. Based on these screening results, they designed and synthesized three indoline-conjugated porphyrins: **CM-a**, **CM-b**, and **CM-c** (Fig. 4). As they expected, the molar extinction coefficients (ε) of the Soret and Q-bands for **CM-a**, **CM-b**, and **CM-c** were larger than those for **YD2-*o*-C8**, indicating the improvement of the light-harvesting abilities. Although the dye-loading amounts (Γ) for **CM-a** (2.1×10^{-7} mol cm^{-2}), **CM-b** (1.4×10^{-7} mol cm^{-2}), and **CM-c** (1.5×10^{-7} mol cm^{-2}) were smaller than that for **YD2-*o*-C8** (3.9×10^{-7} mol cm^{-2}), which may result from the increasing nonplanarity and rigidity of the indoline unit compared to the diarylamino group of **YD2-*o*-C8**, their improved light-harvesting abilities compensated for their smaller dye-loading amounts. Consequently, the maximum PCEs for **CM-a** (8.5%), **CM-b** (10.7%), and **CM-c** (9.7%) were comparable or higher than that for **YD2-*o*-C8** (8.5%). The highest PCE for **CM-b** could be attributed to its strongest absorption of both Soret and Q-bands. This value was a record for non-ruthenium iodine-based DSSCs without a co-sensitizer and co-adsorbate at that time.

In addition to examining the effect of a donor moiety, the effect of an anchoring moiety in the electron-withdrawing group

Table 2 Photovoltaic parameters of porphyrin-based DSSCs with $[Co(bpy)_3]^{2+/3+}$ as the redox shuttle, under simulated AM 1.5 G full sun illumination (input power was 100 mW cm^{-2} without additional illumination)

Dye	J_{SC} (mA cm^{-2})	V_{OC} (V)	F. F.(fill factor)	PCE (%)	Ref.
YD2-*o*-C8[a]	17.3	0.965	0.71	12[e]	17
SM315	18.1	0.91	0.78	13[e]	18
GY50[a]	18.53	0.885	0.773	12.7[e]	19
SGT-021[b]	17.5	0.910	0.753	12.0	20
SGT-020[b]	15.8	0.864	0.766	10.5	20
SM315[b]	16.4	0.893	0.794	11.6	20
YD2-*o*-C8HA[c]	10.0	0.83	0.77	6.4	31
YD2-*o*-C8	12.6	0.88	0.74	8.3	31
ZnPTC[c]	8.46	0.757	0.760	4.87	33
YD2-*o*-C8	14.6	0.912	0.746	9.93	33
ZnEP1[c]	11.1	0.77	0.69	5.9	57
ZnEP2[c]	8.2	0.77	0.64	4.0	57
ZnBD1[c]	13.1	0.78	0.68	7.1	58
ZnBD2[c]	14.1	0.83	0.69	8.2	58
ZnPH1[c]	10.8	0.77	0.69	5.7	58
ZnPH2[c]	7.8	0.76	0.64	3.8	58
ZnPV1[c]	12.2	0.77	0.70	6.6	58
ZnPV2[c]	10.7	0.78	0.64	5.3	58
WW-3	9.81	0.744	0.767	5.6	67
WW-4	3.00	0.500	0.299	0.3	67
DfZnP[c]	14.9	0.798	0.739	8.78	68
DfZnP-*i*Pr[c]	16.6	0.823	0.737	10.1	68
DfZnP-*i*Pr[d]	17.0	0.850	0.740	10.7	68
GY50	16.3	0.874	0.700	10.0	68
GY50[d]	14.5	0.908	0.713	9.42	68
***m*-ZnPD**	12.8	0.821	0.755	7.91	77
YD2-*o*-C8	15.1	0.908	0.738	10.1	77
mSJ1	10.551	0.833	0.762	6.69	86
mSJ2	5.468	0.845	0.752	3.48	86
mSJ3	3.729	0.814	0.768	2.33	86
bSJ1	12.525	0.823	0.779	8.03	86
bSJ2	16.856	0.849	0.759	10.7[e]	86
bSJ3	16.483	0.836	0.755	10.4[e]	86
YD2-*o*-C8	15.130	0.849	0.765	9.83	86

[a] 99.5 mW cm^{-2}. [b] Coadsorbed with **HC-A4** (Fig. 19). [c] Coadsorbed with **CDCA**. [d] Co-sensitized with **LEG4** (Fig. 12). [e] Corrected on the basis of significant figures.

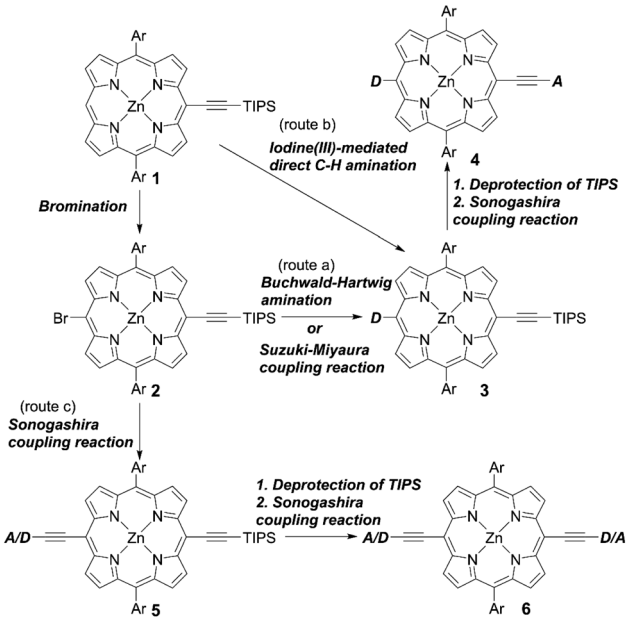

Scheme 1 Synthetic strategies for *meso*-functionalized D–π–A structured porphyrins. Ar = aryl substituents.

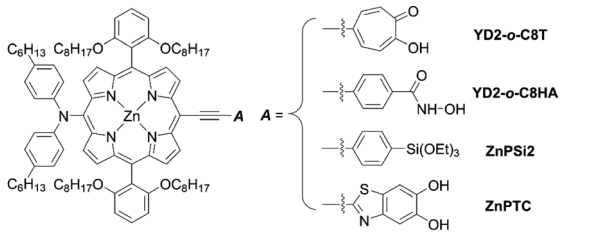

Fig. 5 Chemical structures of representative D–π–A type porphyrins with different anchoring groups.

can be also easily discussed by this synthetic protocol. On the basis of the benchmark dye **YD2-*o*-C8**, Imahori and co-workers designed and synthesized a series of porphyrin dyes, namely **YD2-*o*-C8T** (ref. 30), **YD2-*o*-C8HA** (ref. 31), **ZnPSi2** (ref. 32), and **ZnPTC** (ref. 33) (Fig. 5), by introducing tropolone, hydroxamic acid, triethoxysilyl, and thiazolocatechol moieties, respectively. The PCE values based on these dyes were in the order: **YD2-*o*-C8T** (7.7%) > **YD2-*o*-C8HA** (6.4%) > **ZnPTC** (4.87%) ≈ **ZnPSi2** (4.7%). Although the PCEs for **ZnPSi2** and **ZnPTC** were significantly lower than that for the carboxylic acid dye **YD2-*o*-C8** (7.7–9.93%), the PCEs for **YD2-*o*-C8T** and **YD2-*o*-C8HA** were close to that for **YD2-*o*-C8** (8.3–8.8%). The tropolone anchoring group showed superior long-term durability for iodine-based DSSCs, but it could not be applied to cobalt-based DSSCs due to the too-strong-coordination ability of the tropolone moiety to metal ions. On the other hand, the hydroxamic acid anchoring group was applicable to cobalt-based DSSCs and could attain high long-term durability. In addition, the PCE of 4.7% obtained by a **ZnPTC**-based DSSC is the record efficiency ever reported for DSSCs with catechol-based sensitizers, which had previously never exceeded a PCE of 2%. Generally, the stability of sensitizers, especially the excited state of sensitizers, play the critical role in the durability of DSSCs.[34] Apart from the inherent nature of dyes, the binding ability of the anchoring groups also has a considerable effect on the long-term durability of DSSCs, which is regarded as a reason for the low durability of porphyrin-based DSSCs compared to ruthenium-based counterparts. This is because most porphyrin sensitizers possess only one carboxyl anchoring group, whereas ruthenium-based dyes typically have at least two carboxyl anchoring groups.[35,36] For instance, the representative porphyrin-based dye **SM315** exhibit good long-term durability and is not prone to degradation under continuous irradiation, whereas the desorption of a small amount of dyes results in a slightly decreased PCE. Therefore, stronger anchoring groups are expected to be developed for further improving device durability.

Besides, the iodine(III)-mediated direct C–H amination reaction[37] of the *meso*-free porphyrin **1** and subsequent deprotection and Sonogashira coupling reactions of **3** can be an alternative method to synthesize *trans*-A_2BC-type push–pull porphyrin dyes **4** (Scheme 1, route b). Compared to the Pd-catalyzed reactions of halogenated porphyrins (Scheme 1, route a), adopting the iodine(III)-mediated direct C–H amination reaction can reduce the number of synthetic steps and improve the overall reaction yield. Moreover, the conditions for this reaction are mild (*i.e.* there is no need for a dry solvent or nitrogen atmosphere) and the process is rapid, which can save time and economic costs. Recently, Zheng and co-workers[38] first introduced triptycene groups at the diphenyl amine unit of **YD26** to synthesize **JY74**, as well as **JY75** (Fig. 4) with a BTD auxiliary electron-withdrawing acceptor. As mentioned above, the direct C–H amination simplified the synthetic steps and improved the yield compared with the process requiring the synthesis of a precursor for **YD26** (70% *vs.* 54% for the optimized steps) (Fig. 4, **3** in Scheme 1, Ar = 2,6-di(octyloxyphenyl), D = diphenylamino).[39] **JY75** exhibited a moderate PCE of 6.77%, which was increased by 26.8% and 7.6% compared to those of **YD26** (5.34%) and **JY74** (6.29%), respectively. Because of the well-known rigid and shape-persistent structure of triptycene, its inherent steric effect prevented penetration of the redox shuttle to the surface of TiO_2 efficiently. Furthermore, the introduction of the electron-withdrawing BTD unit further enhanced the J_{SC} value, resulting in the obvious improvement in device efficiency.

Incorporating an additional ethynyl group into the donor side is a useful strategy for enlarging the π-conjugation to overcome the insufficient absorption of porphyrins around 500 nm and over 600 nm. Instead of the Buchwald–Hartwig amination or Suzuki–Miyaura coupling reaction, the Sonogashira coupling reaction of **2** and subsequent deprotection and Sonogashira coupling reaction of **5** could furnish the push–pull porphyrin dyes **6** with two ethynyl moieties (Scheme 1, route c). This strategy was established by Lin *et al.* for the synthesis of **LD13** (Fig. 6).[40] According to this protocol, Xie and co-workers synthesized various D–π–A-type porphyrin sensitizers with red-shifted Q-bands.[41–44] They evaluated the effects of the donor and/or acceptor moieties and found that the introduction of suitable donors and/or acceptors could broaden the absorption band due to the enlarged π-conjugation and strengthened ICT process, resulting in improved device efficiency. Importantly, the introduction of bulky alkyl chains was able to supress dye aggregation and CR caused by the large π-conjugation framework, and further optimize the cell performance. In 2018, Xie and co-workers[45] reported a series of porphyrin sensitizers **XW29–XW32** (Fig. 6) with indoline derivatives as the donor moieties. For **XW29** and **XW31** without the additional BTD acceptor, high PCEs exceeding 10% were attainable. Furthermore, a high PCE of 10.46% was observed by **XW31**, in comparison with that of 10.14% for **XW29**. Both the J_{SC} and V_{OC} values for **XW31** could be improved by introducing the dialkylfluorene unit, as a result of its red-shifted absorption, increased dye-loading amounts, and suppressed CR processes. Specifically, dialkylfluorene-substituted ones (**XW31**: 1.14×10^{-7} mol cm^{-2}, **XW32**: 1.67×10^{-7} mol cm^{-2}) exhibited slightly higher dye-loading amounts than the methylphenyl-substituted analogues (**XW29**: 9.7×10^{-8} mol cm^{-2}, **XW30**: 1.49×10^{-7} mol cm^{-2}), respectively, which may be attributed to the increased dye solubility and promoted dye adsorption process by the additional alkyl chains.[46] However, **XW30** and **XW32** with the additional BTD group afforded lower PCEs of 8.68% and 8.82%, respectively, although they showed higher dye-loading amounts compared to **XW29** and **XW31**. This trend could be explained

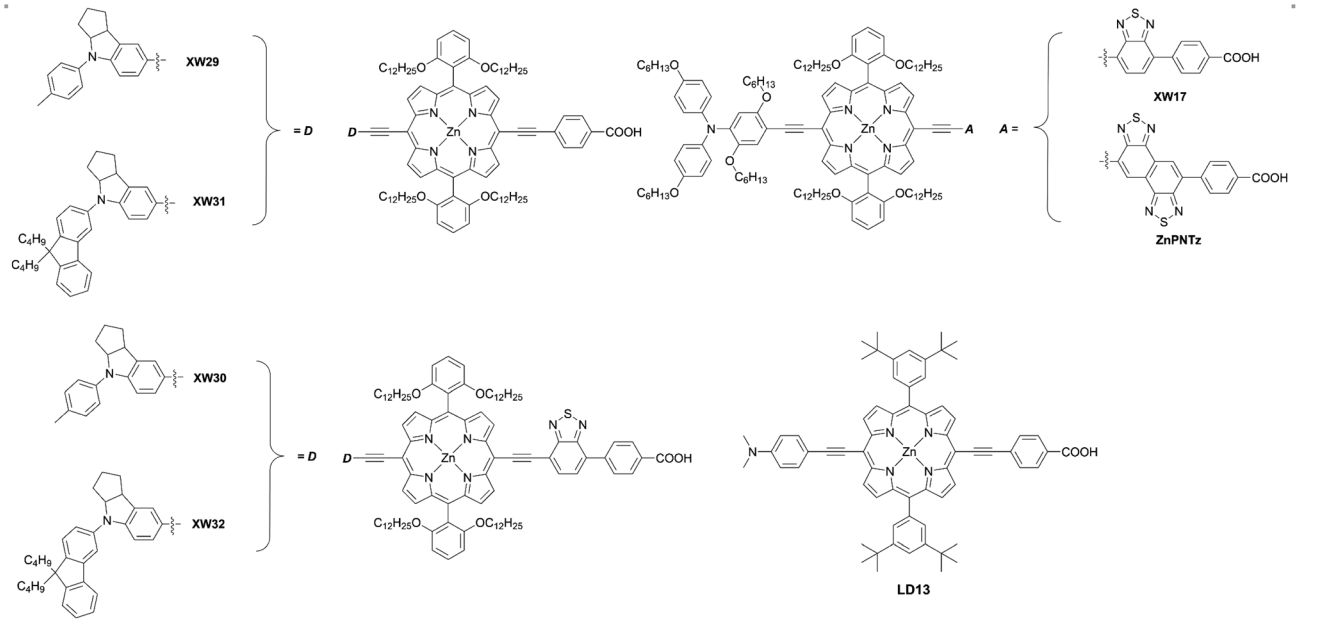

Fig. 6 Chemical structures of representative *meso*-functionalized D–π–A type porphyrins with an acene bridge.

through the increase in their dye aggregation, consistent with the higher Γ values, and charge-recombination effects owing to the introduction of the strong electron-drawing BTD moiety. As we demonstrated before,[47–49] adsorbed Zn-porphyrins on TiO_2 are heavily tilted to the surface, even if they are well-packed on TiO_2 (40°∼70° from the surface normal). The tilt angle of Zn-porphyrins on TiO_2 depends on the dye-loading amount, molecular length, bulkiness, interaction between specifically incorporated atoms (N, F, S atoms) and TiO_2, and the adsorption conditions (time, immersion solvent, *etc.*). Thus, electron transfer (ET) between the porphyrin and TiO_2 occurs through a through-space mechanism rather than a through-bond mechanism. Namely, a greater tilted geometry of the porphyrin on TiO_2 leads to faster electron injection from the excited porphyrin to TiO_2 and faster CR from TiO_2 to the oxidized porphyrin, thus lowering the PCE. Overall, this trend mentioned above can be rationalized by plausible fast CR in **XW30** and **XW32** due to their longer molecular lengths and resultant more tilted adsorption orientation on TiO_2. Meanwhile, Imahori and co-workers[50] first introduced the naphtho-[1,2-*c*:5,6-*c*′]bis[1,2,5]-thiadiazole (NTz) unit into porphyrins-based DSSCs (**ZnPNTz**) (Fig. 6). The stronger electron-withdrawing ability of the NTz moiety than the widely used BTD was expected to enhance the light-harvesting ability. In comparison with **XW17** (Fig. 6),[43] **ZnPNTz** showed a red-shifted (14 nm) and broadened Q-band, and the absorption edge exceeded 800 nm. However, a lower PCE of 3.63% was observed for **ZnPNTz** than that for **XW17** (8.14%). The lower PCE of **ZnPNTz** may have resulted from the inefficient electron injection derived from its inferior ET parameters as well as much faster CR, as a result of the longer molecular length of **ZnPNTz** than that of **XW17**.[47–49]

In contrast to *trans*-A_2BC-type push–pull porphyrin dyes, *cis*-A_2BC-type push–pull porphyrin dyes with two donor moieties are more appealing because of the more favourable orbital distribution in the highest occupied molecular orbital (HOMO) and lowest unoccupied molecular orbital (LUMO) for ET processes as well as improved light-harvesting ability by their asymmetrical molecular structure (*vide infra*). Despite the prospect of *cis*-A_2BC-type push–pull porphyrin dyes, it is a synthetic challenge to introduce three different substitutions at desired *meso*-positions. In 2013, Imahori and co-workers first reported the *cis*-A_2BC-type push–pull porphyrin dyes **ZnPBA** and **ZnPBAT** (Fig. 7).[51] First, 5-substituted porphyrin **7** was employed as the starting material. The bromination of the free base porphyrin **7** afforded two isomers of the mono-brominated porphyrins, **8a** and **8b**, which could be separated by conventional silica-gel column chromatography. After the metalation of **8a**, the Sonogashira coupling reaction of **9** provides **10**. Then, bromination and Buchwald–Hartwig coupling reactions, or a iodine(III)-mediated direct C–H amination reaction, gave the corresponding *cis*-A_2BC-type porphyrins **11**. Finally, deprotection of the TIPS moiety, followed by the Sonogashira coupling reaction and hydrolysis furnished the *cis*-A_2BC-type push–pull porphyrin dyes **12** with the two diarylamino moieties (Scheme 2). They synthesized **ZnPBAT** according to this protocol. The reference **ZnPBA** can be prepared by a direct C–H

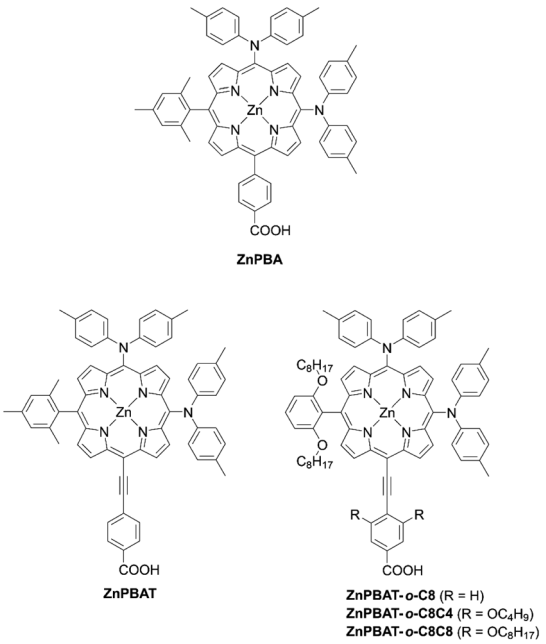

Fig. 7 Chemical structures of representative *cis*-A_2BC-type D–π–A type porphyrins.

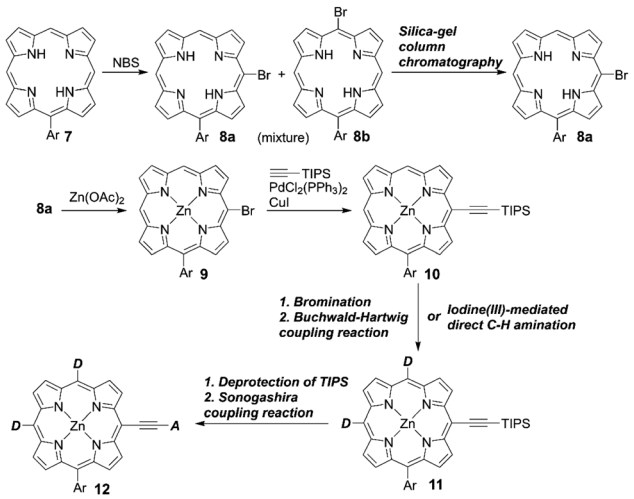

Scheme 2 Synthetic strategy for *cis*-A_2BC-type porphyrins. Ar = aryl substituents; NBS = *N*-bromosuccinimide.

amination of the *cis*-AB-type porphyrin **15** and subsequent hydrolysis and metalation of **16**, which could be obtained by the acid-catalyzed condensation of *meso*-free tripyrrane **13** and metalation of **14** (Scheme 3). Both **ZnPBA** and **ZnPBAT** revealed broadened and red-shifted absorption spectra relative to **YD2** as a result of the introduction of the additional diarylamino moieties. In addition, the Q-bands of **ZnPBAT** were red-shifted compared to **ZnPBA** due to an effective π-extension by the triple bond. Because of the improved light-harvesting ability of **ZnPBAT**, the DSSC with **ZnPBAT** achieved the highest incident photon-to-current efficiency (IPCE) and resulted in the best PCE among these three dyes (**ZnPBA** (8.3%) < **YD2** (9.1%) < **ZnPBAT**

(10.1%)). Moreover, a **ZnPBAT**-based cell exhibited long-term durability and only a 10% decay of the overall device efficiency under exposure to full sunlight for 300 h at 25 °C, which may be attributed to the loss of the volatile solvent in the electrolyte solution and desorption of the sensitizers. Later, Imahori and co-workers further attempted to optimize its molecular structure by introducing alkoxyl groups into the electron-withdrawing anchoring group and *meso*-phenyl group, giving **ZnPBAT-*o*-C8**, **ZnPBAT-*o*-C8C4**, and **ZnPBAT-*o*-C8C8** (Fig. 7).[52] Although the introduction of the alkoxy groups reduced dye aggregation and enhanced the blocking effect effectively, they caused intermolecular alkoxy–alkoxy interactions, resulting in an unexpected aggregation tendency on TiO_2. Additionally, the number of alkoxy chains at the *meso*-substituted benzene rings had a significant effect on the Γ values [**YD2-*o*-C8** (7.9×10^{-11} mol cm^{-2}) < **ZnPBAT-*o*-C8C4** = **ZnPBAT-*o*-C8C8** (8.7×10^{-11} mol cm^{-2}) ≈ **ZnPBAT-*o*-C8** (8.8×10^{-11} mol cm^{-2})]. Note that the Γ values reported by Imahori and co-workers were estimated taking into account the actual surface area of TiO_2 particles in a porous TiO_2 film instead of the projected area of the TiO_2 film. Overall, the PCEs of these four dyes were in the order: **ZnPBAT-*o*-C8C8** (7.0%) < **ZnPBAT-*o*-C8C4** (7.3%) < **YD2-*o*-C8** (8.6%) < **ZnPBAT-*o*-C8** (9.1%).

2.2 β-Functionalized porphyrins

Opposite from *meso*-substituted porphyrins, β-substituted porphyrin dyes are still limited due to their synthetic difficulties in lower symmetry porphyrins. Nevertheless, many efforts have been directed towards developing β-functionalized push–pull porphyrins. Generally, β-brominated or β-borylated porphyrins are key precursors because a variety of substituents can be introduced by transition metal-catalyzed coupling reactions. In 2013, Pizzotti and co-workers[53] reported a series of β-mono-substituted (**23–25**, Fig. 8) or disubstituted push–pull *meso*-tetraarylporphyrins (**21** and **22**, Fig. 8). As illustrated in Scheme 4, the β-brominated intermediates **18a** and **18b** were synthesized from **17** by β-bromination with NBS. Then, the Sonogashira coupling reactions of **18a** and **18b** provided the β-functionalized porphyrins **19** and **20**, respectively. Although *meso*-substituted analogues **26–28** (Fig. 8) exhibited lower HOMO–LUMO energy gaps, the β-monosubstituted or disubstituted ones showed comparable or better device performance, which were in accordance with their enhanced IPCE spectra. Among **21–28**, dye **22** with a cyanoacrylic acid as the anchoring group and *N*,*N*-dimethylaminophenylethynyl moiety as the

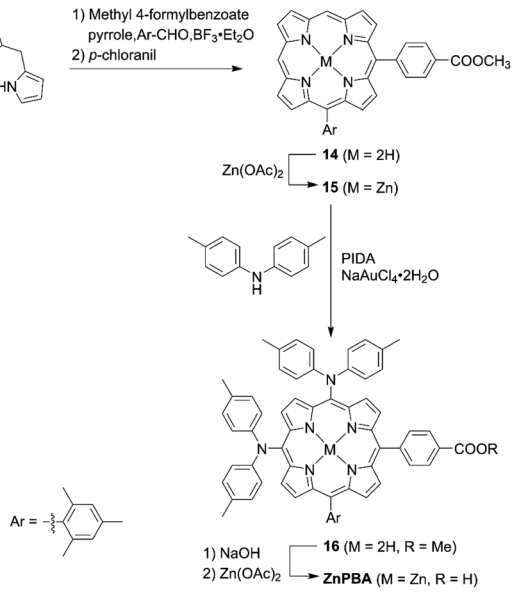

Scheme 3 Synthesis of **ZnPBA**. PIDA = phenyliodine(III) diacetate.

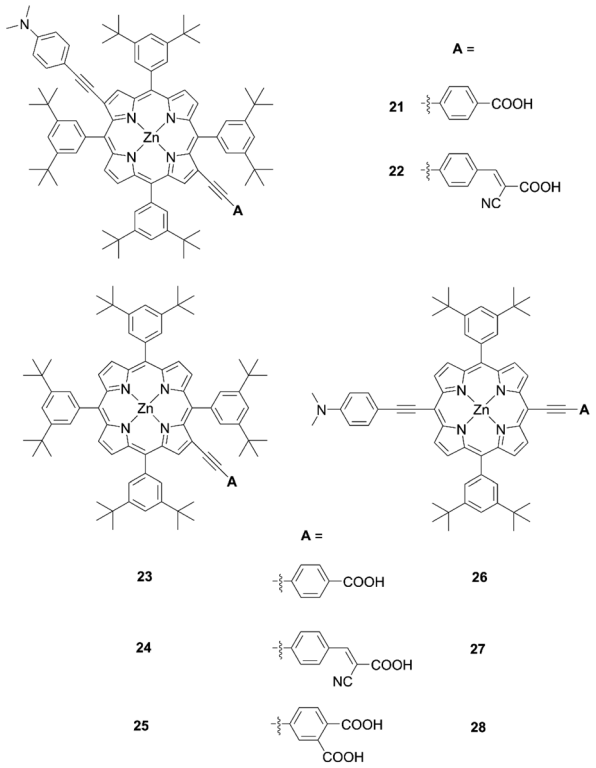

Fig. 8 Chemical structures of **21–28**.

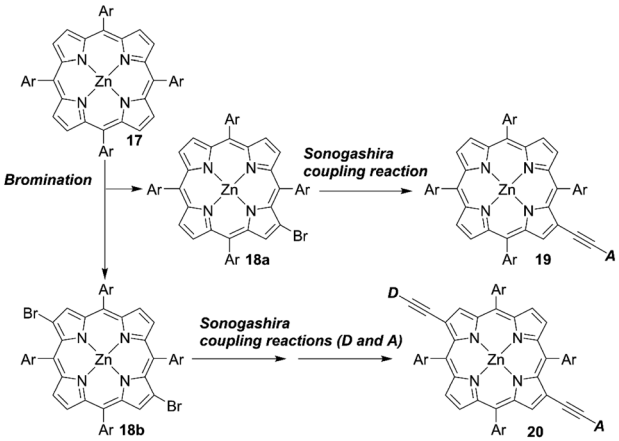

Scheme 4 Synthetic strategies for β-functionalized D–π–A-type porphyrins. Ar = aryl substituents.

donor group gave a moderate PCE of 4.7%. The higher PCE may originate from the localization of the LUMO in the electron-withdrawing anchoring group and that of the HOMO in the electron-donating group, which would accelerate electron injection from the dye to TiO_2 and slow down CR between the dye radical cation and TiO_2.

Yeh and co-workers[54] prepared the β-dibrominated porphyrin precursor **34** by an acid-catalyzed condensation of the corresponding dipyrromethanes **32** and **33** and subsequent oxidization by 2,3-dichloro-5,6-dicyano-1,4-benzoquinone (DDQ) (Scheme 5). The Grignard reagent-mediated acylation of dipyrromethane **29** with 3,5-di-*tert*-butylbenzoyl chloride afforded the diacyldipyrromethane **30**. After the bromination of **30**, the reduction of **31** with $NaBH_4$ yielded the key bis(hydroxymethyl)dippyromethane **32**. After the metalation of **34**, the Buchwald–Hartwig amination of **35** furnished the β-aminoporphyrin **36**. Deprotection of the TIPS moiety and a subsequent Sonogashira coupling reaction gave the porphyrin dye **SK7** (Scheme 5). These reactions are notable as they show that the β-dibromoporphyrins **34** and **35** may become key precursors for various β-difunctionalized porphyrin sensitizers. The introduction of two amino groups at the β-positions can have a considerable impact on the a_{1u} orbital but not the a_{2u} orbital, which leads to a decrease in the degeneracy of HOMO/HOMO−1. Consequently, the Soret band of **SK7** appeared as two split peaks (λ_{max} = 424, 491 nm), which made up for the weak absorption of typical porphyrins around 450–550 nm and thereby enhance the light-harvesting ability. However, the dye-loading amount for **SK7** (6.08×10^{-8} mol cm^{-2}, where the thickness of TiO_2 was 15 μm, which was the same as for **YD2**) was two-thirds of that for **YD2** (9.48×10^{-8} mol cm^{-2}) (Fig. 4). The lower dye-loading amount was responsible for the lower J_{SC} value (13.25 *vs.* 15.42 mA cm^{-2}) and resultant lower PCE (6.54% *vs.* 7.78%) under 1 sun illumination. Although **SK7** possessed two bulky diarylamino groups, a loose packing of **SK7** on TiO_2 was obtained under the T5 light source, but the PCE of the **SK7**-based device was nearly 97% that of **YD2** (84% under 1 sun). This could be rationalized by the much more matched emission wavelengths of the incident light sources.

Osuka and co-workers[55] presented a highly regioselective C–H borylation reaction of *meso*-arylporphyrins using an iridium catalyst. Inspired by this work, Sessler, Kim, and co-workers designed several β-functionalized porphyrins with the *meso*-diarylamino group.[56,57] As illustrated in Scheme 6, the borylation reaction of *meso*-aminoporphyrin **37** yielded a mixture of the mono- or bis-borylated porphyrins **38a** and **38b**. Then, acceptor moieties were introduced by transition metal-catalyzed coupling reactions to give the D–π–A-type porphyrins **39a** and **39b**. Especially, they developed a process for the direct palladium-catalyzed oxidative alkynylation of β-borylated porphyrins, instead of going *via* a common bromo-precursor, for the preparation of push–pull-structured ethynylbenzoic acid porphyrin derivatives. Although the nature of the terminal alkynes had a considerable effect on the reaction yield (*i.e.* electron-deficient alkynes were less reactive than electron-rich ones), the simplified synthetic routes, *i.e.* omitting the bromination of β-borylated porphyrins, were beneficial for improving the overall yield and synthetic costs. Initially, **ZnBD1** and **ZnBD2** (Fig. 9) achieved moderate efficiencies of 5.9% and 7.5% with the I^-/I_3^- redox couple, respectively.[56] After optimization with a cobalt-based electrolyte, **ZnBD2** attained a record PCE of 8.2% among doubly β-butadiene-linked porphyrin sensitizers for DSSCs.[58] The introduction of additional β-linkages gave rise to a red-shifted and broadened absorption spectrum for **ZnEP2** compared to **ZnEP1** (Fig. 9). Despite its enhanced light-harvesting ability, the **ZnEP2**-based DSSC exhibited a lower PCE (4.0%) than that of the **ZnEP1**-based DSSC (5.9%). The lower PCE for **ZnEP2** was attributed to the lower *J*sc value, which may be rationalized by the low dye-loading amount (*ca.* one-

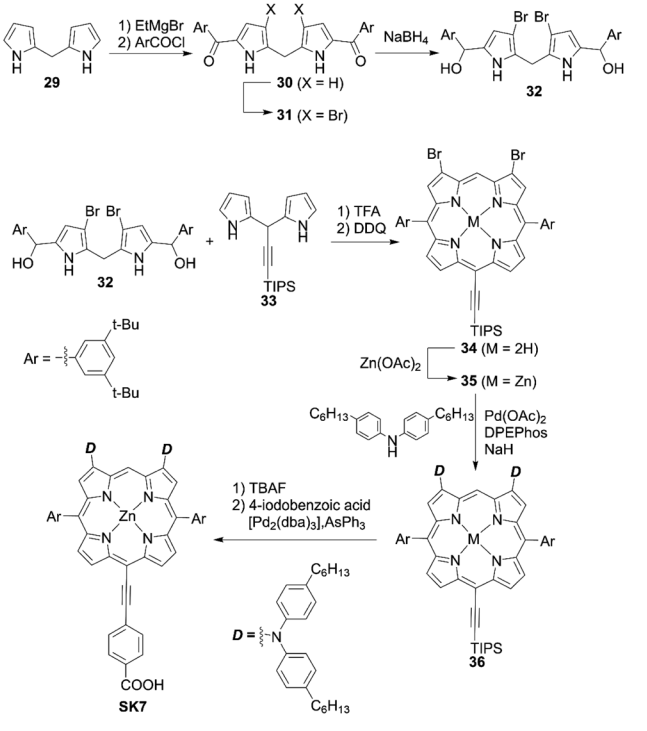

Scheme 5 Synthesis of **SK7** with two donor moieties at β-positions. TFA = trifluoroacetic acid; DPEPhos = bis[(2-diphenylphosphino) phenyl]ether; $[Pd_2(dba)_3]$ = tris(dibenzylideneacetone)dipalladium(0).

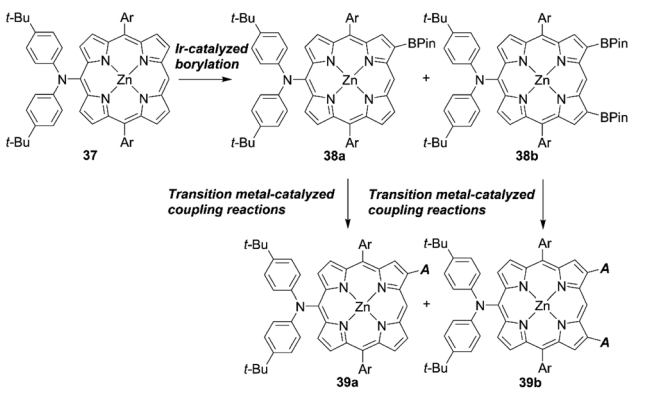

Scheme 6 Synthetic strategies for β-functionalized porphyrins *via* Ir-catalyzed borylation. Ar = aryl substituents.

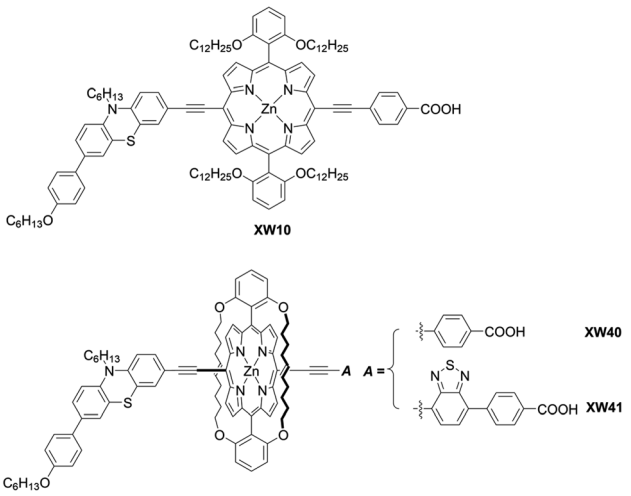

Fig. 9 Chemical structures of ZnBD1-2, ZnPH1-2, and ZnPV1-2.

third) relative to **ZnEP1**. Moreover, the dihedral angle between the porphyrin core and the ethynylphenyl rings was larger in **ZnEP2** (17.4°) than that in **ZnEP1** (0.7°) with the optimized structures. The larger dihedral angle could disrupt the effective electronic communication through the ethynylphenyl π-bridge and retard efficient electron injection. Considering the importance of the rigidity of the two anchoring groups in the photovoltaic performance, they synthesized a series of new β-functionalized push–pull-type porphyrins (**ZnPHn** and **ZnPVn**: n = 1 and 2, Fig. 9).[58] The DSSCs with **ZnPHn** bearing the rigid π spacer provided lower PCEs than those with **ZnPVn**. The low light-harvesting abilities of **ZnPHn** were mainly responsible for the decreased J_{SC} values.

Furthermore, the dihedral angles between the β-aryl rings and porphyrin core of **ZnPHn** were *ca.* 43°, which led to a weak electronic coupling between the LUMO of **ZnPHn** and the CB of TiO_2 as well as between the acceptor moiety and porphyrin core. Consequently, the ϕ_{inj} values may become lower for **ZnPHn** than those for **ZnPVn**. In contrast, the dihedral angles between the carboxyphenyl rings and porphyrin core were significantly small for **ZnPVn**, which enabled strong electronic coupling between the acceptor moieties and porphyrin core. This efficient electronic communication resulted in large orbital distributions on the acceptor moiety of LUMO, leading to the high ϕ_{inj} values. Furthermore, the CR from the CB of TiO_2 was expected to be slower over a longer distance as a result of the C=C double bond π-spacer. Therefore, the DSSCs with **ZnPVn** exhibited higher PCEs than those with **ZnPHn**. These studies indicated that the flexible and small alkenyl π-conjugated spacers play an important role in the molecular structures and electron coupling, which offers a valuable guide for rational molecular design.

3. Aromatic-fused porphyrins

The incorporation of an aromatic-fused structure into a porphyrin core is a promising strategy for obtaining highly efficient DSSCs because of the extended π-system and resultant red-shifted absorption. In 2007, Imahori and co-workers[59,60] synthesized a *meso*-naphthyl-fused porphyrin, **fused-Zn-1**, which was the first example of a fused porphyrin-based DSSC. The intermediate **42** could be prepared by the metalation of **40** and successive treatment of the precursor **41** with $FeCl_3$ and TFA. Then, a subsequent hydrolysis and Zn(II)-metalation afforded the target molecule (Scheme 7). Compared to the non-fused counterpart **Zn-1** (Scheme 7), the Soret and Q-bands of **fused-Zn-1** were broadened and red-shifted by ~60 and 130 nm. A higher PCE of 4.1% for the **fused-Zn-1** than that of 2.8% for **Zn-1** was obtained. Then, Imahori and co-workers[61] continued to present the first example of two β,β′-edge quinoxaline-fused zinc porphyrins: **ZnQMA** with a PCE of 5.2% and **ZnQDA** with a PCE of 4.0%. The inferior PCE of **ZnQDA** was mainly due to the lower electron injection and charge-collection efficiency related to the weaker coplanarity of the two carboxylic acid groups with the porphyrin plane and the higher degree of proton transfer from **ZnQDA** to TiO_2 (Scheme 8). The key intermediate **44** could be synthesized by oxidation of the precursor **43** with Dess–

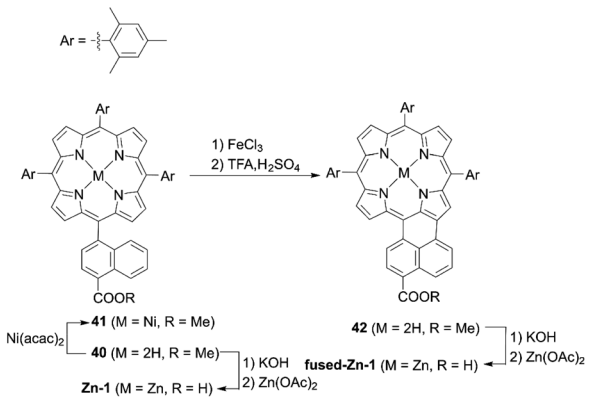

Scheme 7 Synthesis of **fused-Zn-1**. Ni(acac)$_2$ = nickel(II) bis(acetylacetonate).

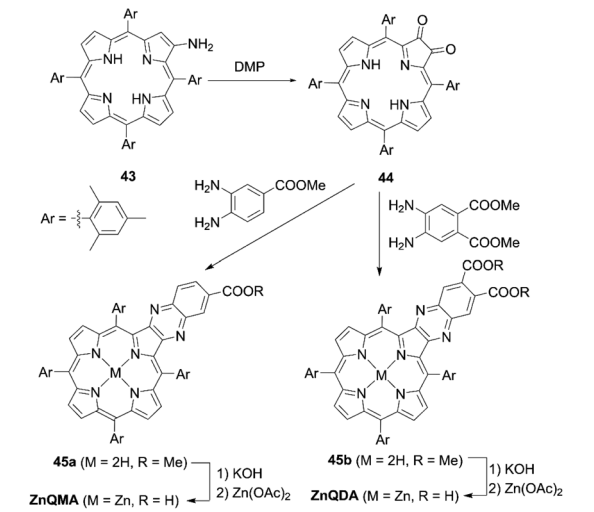

Scheme 8 Syntheses of ZnQMA and ZnQDA.

Martin periodinane (DMP). **ZnQMA** and **ZnQDA** were derived from the condensation of intermediate **44** with the substrates with different numbers of ester groups, followed by the subsequent hydrolysis and metalation reactions of **45a** and **45b**. Later, they reported the fused porphyrin **ZnPQI** (ref. 62) with a push–pull structure. **ZnPQI** could be synthesized through the condensation of **47** with methyl 3,4-diaminobenzoate, followed by the hydrolysis and metalation reactions of **48**, in which **47** was afforded by the acid-catalyzed coupling reaction of intermediate **46** with the corresponding triarylamine (Scheme 9). As expected, the absorption spectrum of **ZnPQI** was further red-shifted. A moderate PCE of 6.8% was obtained by the DSSC with **ZnPQI**. This was slightly higher than that with **ZnQMA**, implying the importance of the push–pull structure even in aromatic-fused porphyrins for DSSCs.

Besides, Imahori *et al.* reported that the simple fusion reaction between the β-position and neighbouring benzene ring with an anchoring carboxylic acid made a fused five-membered porphyrin, **fused-ZnP**, with an absorption edge of 800 nm (Fig. 10).[63] Unfortunately, the PCE (0.30%) was very low, probably due to very fast nonradiative decay of the excited singlet state to the ground state by the directly fused structure.

Other fused porphyrins with larger π-systems were also reported to further enhance the light-harvesting abilities. Wang and co-workers[64] provided an efficient method for the synthesis of functionalized *opp*-dibenzoporphyrin by introducing alkenyl groups to the porphyrin periphery. Their synthetic strategy consisted of the Heck reaction of **49** to generate the intermediate **50**, and subsequent electrocyclization and aromatization reactions to yield **51** in one pot (Scheme 10). This could overcome the drawbacks of most synthetic methods for benzoporphyrins, *i.e.* the lack of functional groups introduced at the fused aromatic rings and the synthetic difficulties because of the fewer purification processes during the one-pot approach.

Then, a series of β-functionalized push–pull zinc *opp*-dibenzoporphyrins were synthesized and applied in DSSCs. In 2019, they designed and synthesized two dibenzoporphyrins:

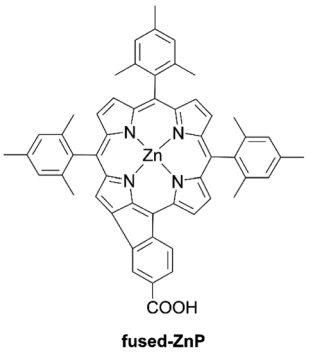

Fig. 10 Chemical structure of **fused-ZnP**.

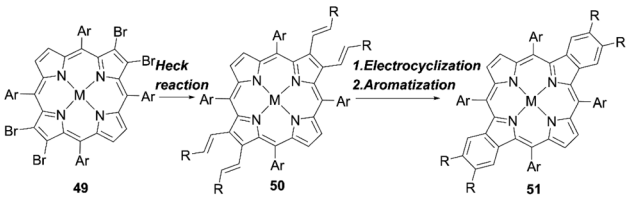

Scheme 10 Synthetic strategy for functionalized *opp*-dibenzoporphyrins. Ar = aryl substituents; M = Ni or Zn; R = phenyl or carbomethoxy.

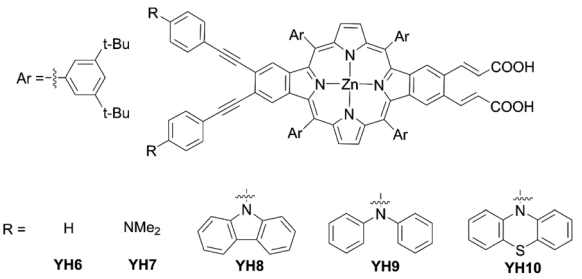

Fig. 11 Chemical structures of YHn (n = 6–10).

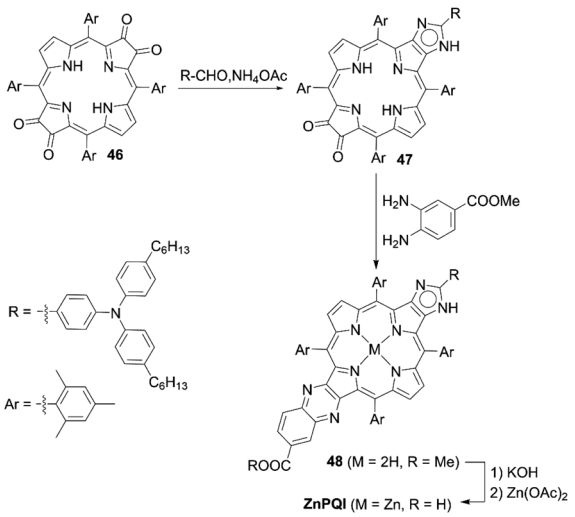

Scheme 9 Synthesis of **ZnPQI**.

YH6 and **YH7** (Fig. 11).[65] **YH7** displayed clearly segregated HOMO/LUMO and fast electron injection owing to the enhanced push–pull character caused by the incorporation of both phenylethynyl bridges and amino groups. However, the non-push–pull porphyrin **YH6** had a higher PCE of 6.70% than that of **YH7** (5.72%), which could be attributed to the illumination-induced photodegradation of **YH7** in the presence of the redox shuttle I^-/I_3^-. They supposed that tertiary amino groups were responsible for this severe photodegradation. They further designed and synthesized dibenzoporphyrin dyes **YH8** with the carbazole moiety, **YH9** with the diphenylamine moiety, and **YH10** with the phenothiazine moiety, in which aliphatic amine was replaced with arylamine (Fig. 11).[66] In contrast to a **YH7**-based device, the **YH8**-**10**-based device revealed good stability similar to **YH6** during the photovoltaic measurement, because the bulky tertiary arylamine protected the amine group from interacting with the redox shuttle on the TiO_2 surface. Moreover, it also benefited from the exceptional light-

harvesting ability allowing **YH9** and **YH10** to yield moderate PCEs of 6.9% and 7.5%, respectively, which were comparable to that (7.7%) of the **N719**-based DSSC. Especially, the reduced CR for the **YH10**-based device contributed to its higher PCE, because the orbital distribution in its HOMO was further away from the TiO_2 surface.

Although fused porphyrins possess extremely enhanced light-harvesting abilities, and some of the absorption edge reach more than 1000 nm, their corresponding DSSCs suffer from the low PCEs stemming from serious dye aggregation, the mismatch of the HOMO–LOMO energy levels, and short lifetimes of the singlet excited-states. For instance, Wu and co-workers[67] presented *N*-annulated perylene (NP)-fused porphyrin **WW-4** (Scheme 11), which was prepared by an $FeBr_3$-promoted intramolecular oxidative cyclodehydrogenation of the precursor **52**, followed by the subsequent Sonogashira coupling reaction of **53**. **WW-4** displayed a maximum absorption at 792 nm (ε = 75 400 M^{-1} cm^{-1}) and two intense absorption bands at 444 nm (ε = 55 200 M^{-1} cm^{-1}) and 540 nm (ε = 69 900 M^{-1} cm^{-1}). However, despite its excellent light-harvesting ability, the **WW-4**-based DSSC showed a much lower PCE of 0.3% than the **WW-3**-based reference (Scheme 11, 5.6%). The low PCE for **WW-4** could be explained by the insufficient driving force for electron injection, caused by its low-lying LUMO energy level (−3.60 eV) in comparison with that of **WW-3** (−3.09 eV).

To surmount the obstacles for aromatic-fused porphyrin dyes, Imahori and co-workers[68] created a series of substituted methylene-bridged thiophene-fused porphyrin sensitizers **AfZnP**, **DfZnP**, and **DfZnP-*i*Pr** (Fig. 12). The substituted methylene-bridged thiophene-fused structure was expected to modulate the electronic communication between the porphyrin core and thiophene moiety, while suppressing the dye aggregation on TiO_2 by the bulkiness around the porphyrin. In the synthetic scheme, *meso*-thienyl porphyrin **54** with an ester moiety on the *meso*-thienyl moiety was a key intermediate. The treatment of **54** with *n*-BuLi afforded the alcohol **55**, which underwent an intramolecular Friedel–Crafts reaction to yield methylene-bridged thiophene-fused porphyrin **56** (Scheme 12).

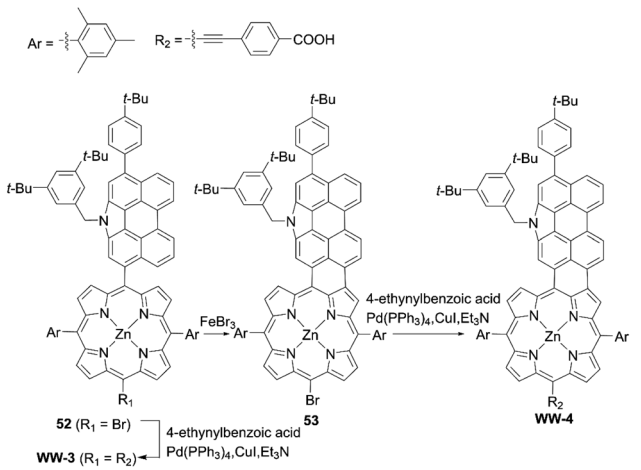

Scheme 11 Synthesis of WW-4.

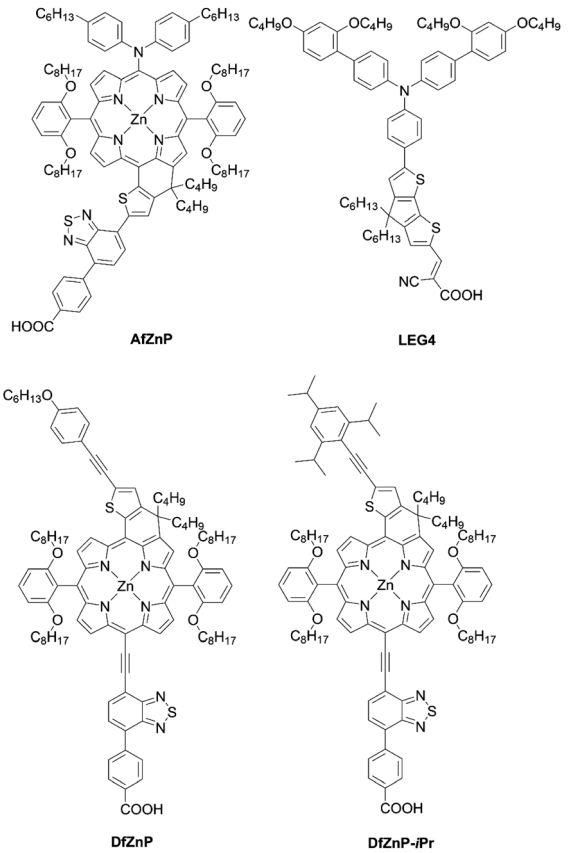

Fig. 12 Chemical structures of AfZnP, DfZnP, DfZnP-*i*Pr, and LEG4.

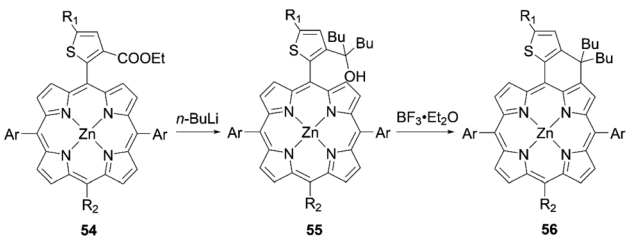

Scheme 12 Synthetic strategy for methylene-bridged thiophene-fused porphyrins. Ar = 2,6-di(octyloxy)phenyl; R_1 = H or alkynyl substituents; R_2 = diarylamino or TIPS group.

It was found that the fusion of thiophene to the porphyrin core on the donor side instead of the acceptor side was more efficient in order to enhance not only its molar extinction coefficients, but also light-harvesting ability. Meanwhile, an increase in the length of the linkers between a porphyrin core and TiO_2 and closer HOMO orbital distribution to TiO_2 by the introduction of the thiophene to the acceptor side would lead to fast CR because of the tilted geometry and close orbital distribution to TiO_2.[47–49] The more tilted geometry also resulted in a lower Γ value of **AfZnP** (**AfZnP** (4.8×10^{-11} mol cm^{-2}) < **DfZnP-*i*Pr** (7.5×10^{-11} mol cm^{-2}) ≈ **DfZnP** (7.6×10^{-11} mol cm^{-2})). Therefore, **AfZnP** bearing the thiophene ring fused on the acceptor side exhibited a lower PCE than those for **DfZnP** and **DfZnP-*i*Pr** containing the fused structure on the donor side. In addition,

the DSSC with **DfZnP-iPr** achieved a promising PCE of 10.1% with the $[Co(bpy)_3]^{2+/3+}$ redox shuttle as a result of the larger steric hindrance and resultant blocking effect on CR between TiO_2 and the redox shuttle by 2,4,6-triisopropylphenyl group. The PCE was comparable with the one for **GY50** (PCE = 10.0%) under the optimized conditions. Remarkably, co-sensitization with the complementary **LEG4** (Fig. 12) further boosted the PCE to 10.7%, a record for fused-porphyrin sensitizers in DSSCs. Such a combination of a push–pull structure, fused structure, and co-sensitization would be a very promising strategy for further enhancing the PCE in DSSCs.

4. Porphyrin dimers

Covalently linked porphyrin dimers have attracted much attention because of their extended π-conjugated systems and excellent light-harvesting abilities arising from the double number and exciton coupling of the porphyrins. Since the first report on porphyrin dimers for DSSCs by Segawa[69] and Officer,[70] various porphyrin dimers for DSSCs have been designed and synthesized. Considering the success of push–pull-type porphyrin dyes, push–pull-type porphyrin dimers are attractive targets for high-performance DSSCs.

Lin and co-workers[71] designed and synthesized an ethynyl-bridged dimeric porphyrin dye **LDD1** based on the D–π–A-type porphyrin **LD14** (Scheme 13), through a Sonogashira coupling between the donor-side porphyrin **57** and the acceptor-side porphyrin **58** and the subsequent hydrolysis reaction of **59**. As expected, **LDD1** revealed a wide absorption spectrum extending beyond 800 nm, but its PCE of 8.8% was lower than that for the **LD14**-based device (9.2%) due to serious dye aggregation. In addition, after the co-sensitization of **LDD1** with **LD14** under the optimized molar ratio, the PCE rose to 10.4% owing to the further improved light-harvesting ability reaching 900 nm. Furthermore, Imahori and co-workers[72] reported the porphyrin dimer **ZnPTD** to replace the two *meso*-phenyl groups with two diarylamino groups on the basis of **LDD1**, expecting there would be an improvement in the light-harvesting ability (Fig. 13). Similarly, the absorption edge of **ZnPTD** was extended up to 900 nm, but the PCE of the DSSC with **ZnPTD** (6.22%) was lower than that with **LDD1** (8.17%). The decrease in the PCE may be ascribed to the more tilted geometry of **ZnPTD** on TiO_2 and thereby the faster CR between the injected electrons in the CB of TiO_2 and the porphyrin radical cation.[47–49] Given that the ethynyl-linked porphyrin dimers exhibit excellent light-harvesting abilities, the suppression of dye aggregation and/or control of dye geometry on TiO_2 by a co-adsorbent/co-sensitizer and/or by the pretreatment of TiO_2 may boost their PCEs.

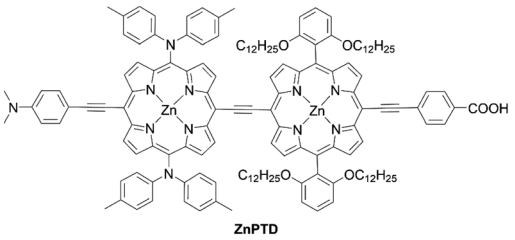

Fig. 13 Chemical structure of ZnPTD.

Zheng and co-workers[73] presented the novel double D–π–A *meso–meso* directly linked porphyrin dimer **JY07** (Scheme 14), which could be synthesized by the treatment of the *meso*-free porphyrin precursor **60** with phenyliodine(III) bis(trifluoroacetate) (PIFA) and the subsequent hydrolysis of **61**. In comparison with the monomer **JY06**, the dimer **JY07** exhibited broader and split Soret bands, as well as red-shifted and enhanced Q-bands due to the strong exciton coupling between the adjacent porphyrins, indicating the improved light-harvesting capability. Besides, the orthogonal conformation of **JY07** suppressed the dye aggregation and CR. Therefore, the dimer **JY07** showed much higher V_{OC} (0.65 V *vs.* 0.63 V) and J_{SC} (13.20 mA cm^2 *vs.* 11.18 mA cm^2) values. As a result, the PCE of 5.33% for **JY07** was larger than the 4.30% for **JY06**. Moreover,

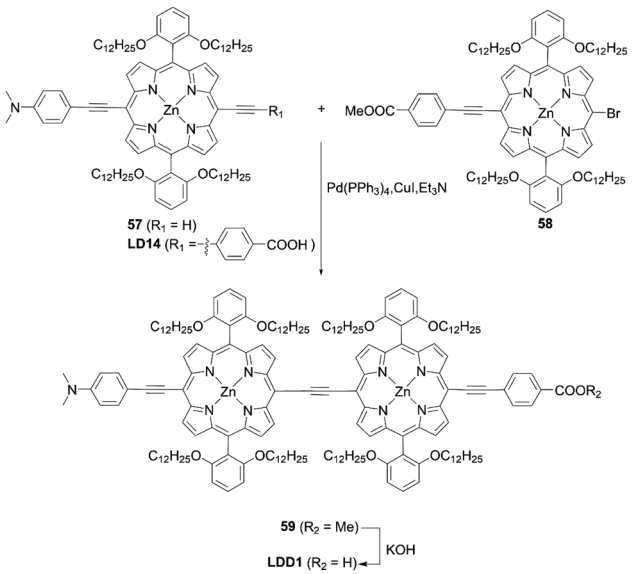

Scheme 13 Synthesis of LDD1.

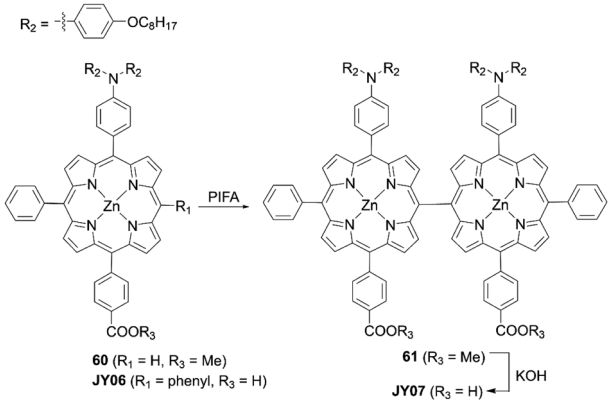

Scheme 14 Synthesis of JY07.

JY07 showed improved photostability due to the presence of two anchoring groups relative to **JY06**.

As observed in the synthesis of **JY07**, the oxidative homocoupling of *meso*-free porphyrins with an oxidant silver hexafluorophosphate ($AgPF_6$)[74,75] or PIFA[76]) is a powerful tool for the synthesis of *meso–meso* directly linked porphyrin oligomers. However, such oxidative homocoupling is mainly limited to the reaction of partially *meso*-aryl porphyrins. Namely, the widely used *meso*-functional substituents (alkynyl and/or amino groups) may not be tolerated. In this context, it is challenging to create a rational synthetic strategy for *meso–meso* directly linked porphyrin dimers suitable for DSSCs. Imahori and co-workers[77] established a general synthetic strategy for ABC–ABC-type *meso–meso* directly linked porphyrin dimers with different substituents at the *meso*-positions. They had previously reported that the bromination of 5-substituted porphyrin afforded two bromoporphyrin isomers, which could be separated by conventional silica-gel column chromatography (see **8a** and **8b** Scheme 2). Accordingly, the borylation of bromo group of **62** and subsequent Suzuki–Miyaura coupling reaction of **63** and demetallation reaction of **64** yielded the *meso*-free porphyrin dimer **65** as a key precursor (Scheme 15). Stepwise regioselective functionalization provided the partially *meso*-free *meso*-AB–AB type porphyrin dimer **67** *via* **66** and **67**; then finally the *meso*-ABC–ABC-type porphyrin dimer ***m*-ZnPD** could be obtained from **68** and **69**. The DSSC with ***m*-ZnPD** reached a record PCE of 7.91% for DSSCs based on orthogonal dimeric D–π–A-type organic sensitizers. This relatively high PCE was mainly attributable to the split Soret bands, red-shifted Q-bands, and resultantly improved light-harvesting ability in the visible and near-infrared regions. Additionally, the strong binding ability from the double anchoring of ***m*-ZnPD** on TiO_2 was beneficial for improving the durability of DSSCs in comparison with the reference **YD2-*o*-C8** with a single anchoring group. However, the rigid orthogonal dimeric structure of ***m*-ZnPD** may form a large void space on TiO_2 that allows the redox shuttle to approach TiO_2, accelerating CR and lowering the PCE relative to **YD2-*o*-C8** (10.1%). It is noteworthy that this general synthetic strategy is applicable to ABC–ABC-type *meso–meso* directly linked porphyrin dimers for various applications.

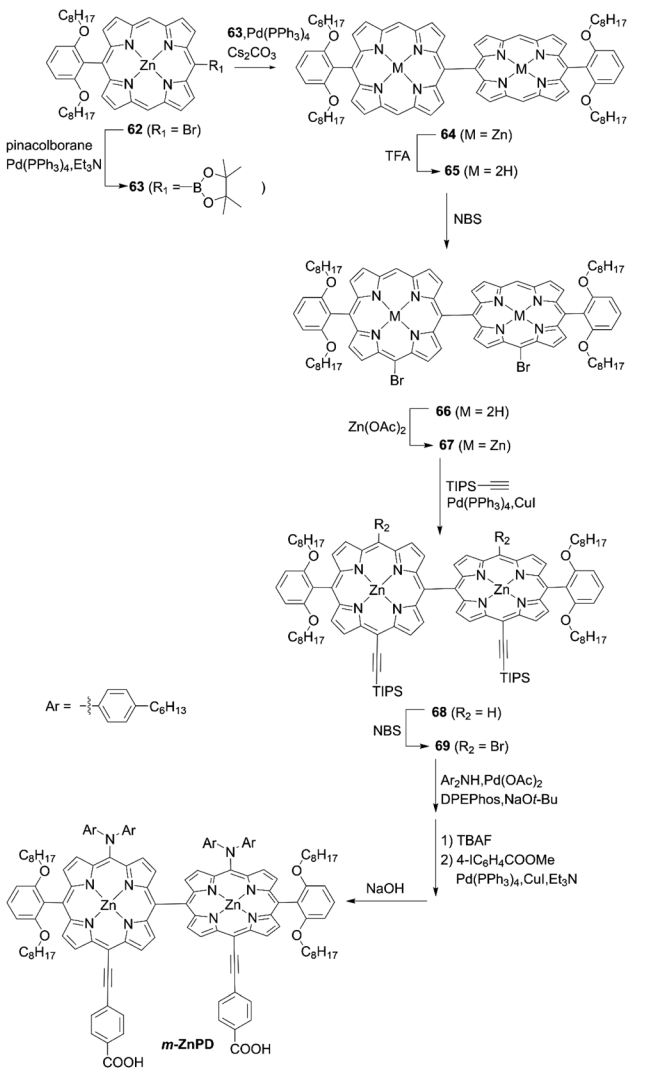

Scheme 15 Synthetic strategy for *m*-ZnPD.

5. Chlorins and bacteriochlorins

Porphyrins have an allowed $S_0 \rightarrow S_2$ transition (Soret band) and a forbidden $S_0 \rightarrow S_1$ one (Q-bands). Lowering the symmetry of porphyrins leads to less allowed $S_0 \rightarrow S_2$ transition and allowed $S_0 \rightarrow S_1$ one, matching better with the solar energy distribution on earth. In this regard, partially hydrogenated chlorin (17,18-dihydroporphyrin) and bacteriochlorin (7,8,17,18-tetrahydroporphyrin) derivatives have attracted considerable interests and are regarded as potential dye sensitizers owing to their excellent light-harvesting abilities at wavelengths >600 nm. Tamiaki and co-workers[78,79] demonstrated the utility of modified chlorophylls or bacteriochlorophylls as dyes in DSSCs. However, it is still a challenge to synthesize chlorins and bacteriochlorins for DSSCs due to their molecular structures with lower symmetry.

Recently, Feng and co-workers[80] synthesized a series of isomeric chlorin-type sensitizers according to the 1,3-dipolar cycloaddition reaction between the free base porphyrin **70** and nitrile oxide, as well as the subsequent metalation and hydrolysis reactions of **71**, **72**, **73**, and **74**, respectively (Scheme 16). They found that the PCEs for **76** (2.92%) and **77** (1.85%) were lower than those for **75** (3.65%) and **78** (3.60%) because of the dye aggregation on TiO_2 and inhibition of dye adsorption onto TiO_2, associated with the steric hindrance by the 2,5-dichlorophenyl group.

Imahori and co-workers[81] introduced the push–pull structure into bacteriochlorin for the first time for DSSCs. The push–pull-type bacteriochlorin **BC2H** is depicted in Scheme 17. The reduction of *meso*-aminoporphyrin **79** with an excess amount of *p*-toluenesulfonyl hydrazide ($TsNHNH_2$) provided the *meso*-amino bacteriochlorin **80**. Subsequent bromination and the Sonogashira coupling reaction then afforded the push–pull structure of **81**. Finally, the hydrolysis reaction gave **BC2H**,

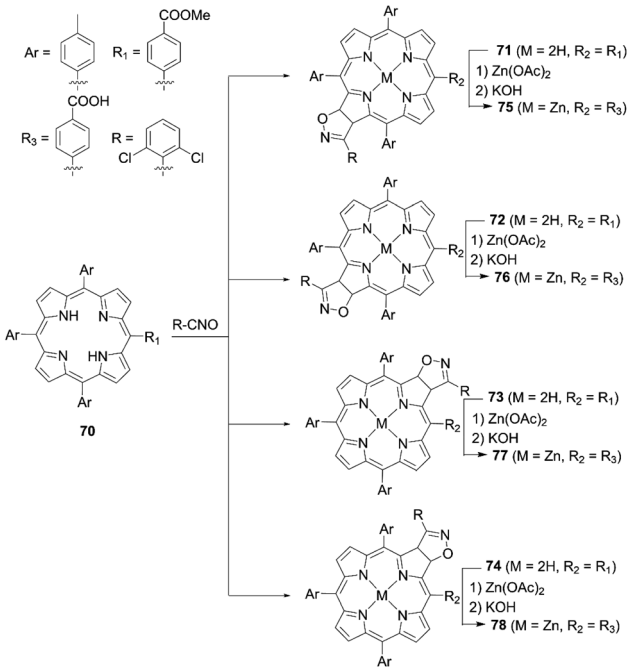

Scheme 16 Syntheses of 75–78.

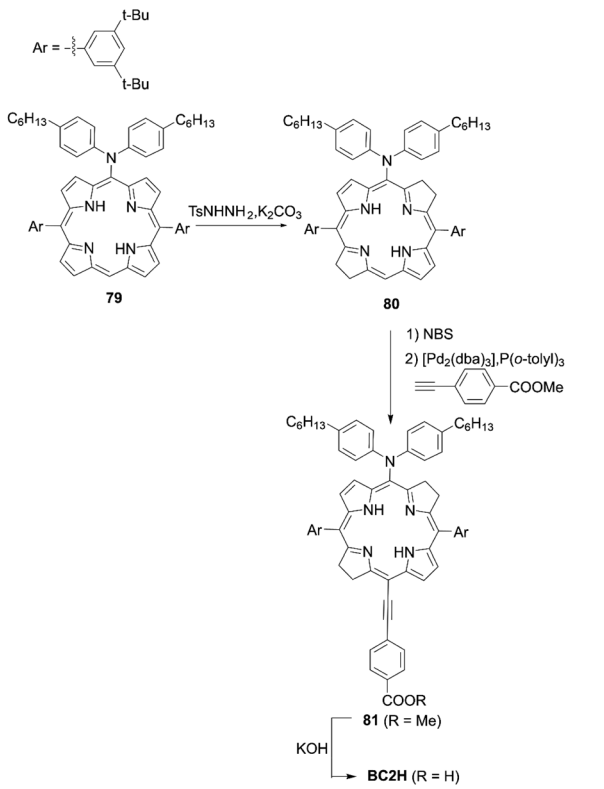

Scheme 17 Synthesis of BC2H. P(*o*-tolyl)$_3$ = tris(*o*-tolyl)phosphine.

showing broad absorption with a wavelength edge of up to 800 nm. Regrettably, the PCE (2.7%) was lower compared to its porphyrin analogue **YD2** (8.9%) under the optimized conditions. The lower PCE was mainly resulted from the serious dye aggregation of **BC2H** on TiO_2, which was consistent with the higher Γ value of **BC2H** (1.0×10^{-10} mol cm^{-2}) than **YD2** (0.9×10^{-10} mol cm^{-2}), and the resultant low ϕ_{inj} value. Nevertheless, it should be noted that **BC2H** revealed excellent stability under an ambient atmosphere, even for several months.

In 2017, Lin and co-workers[82] reported bacteriochlorin-based sensitizers with two geminal dimethyl groups: **LS-01** and **LS-11** (Fig. 14). The key intermediate **82** was prepared by modifying

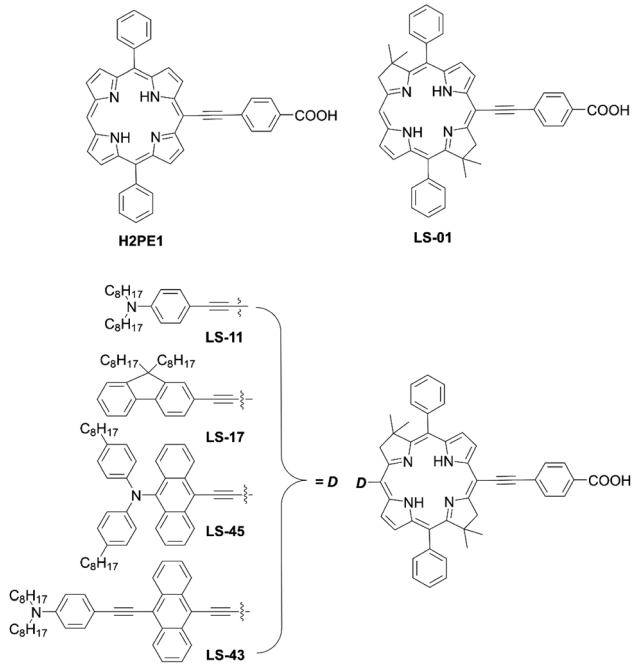

Fig. 14 Chemical structures of H2PE1, LS-01, LS-11, LS-17, LS-43, and LS-45.

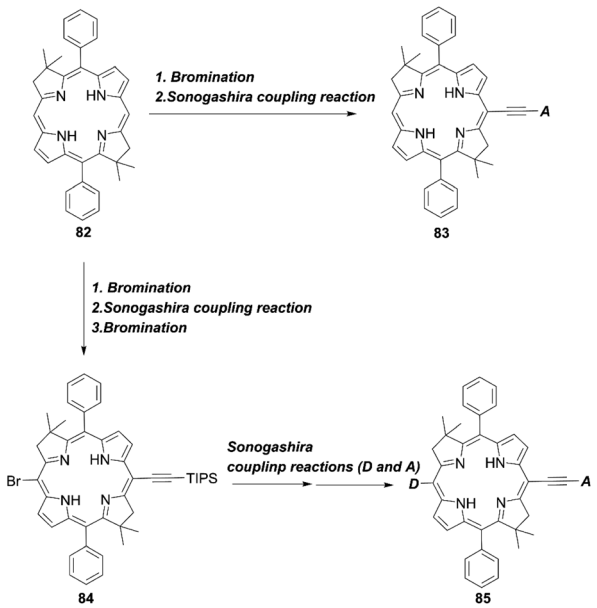

Scheme 18 Synthetic strategy for *meso*-functionalized bacteriochlorins.

the protocol established by Lindsey *et al.*[83] Then, an anchoring group/push–pull structure was introduced by bromination and the Sonogashira coupling reaction of **82**, or a similar synthetic strategy for **82** and **84**, as shown in Scheme 1, route c, to yield **83** and **85** (Scheme 18). As expected, **LS-01** and **LS-11** revealed red-shifted and enhanced Q_x- and Q_y-bands relative to the corresponding porphyrin **H2PE1**, which were useful for the enhanced IPCE and resulted in larger current densities and PCEs (**LS-01** (4.67%), **LS-11** (5.36%), and **H2PE1** (2.06%)). However, in terms of the durability, the **LS** cells exhibited a large decay in device efficiencies compared to the **H2PE1** cell, which may be ascribed to the desorption of dyes on TiO_2 and the resulting decreased J_{SC}. Later, they continued to report three new *meso*-substituted, push–pull bacteriochlorins,[84] coded as **LS-17**, **LS-43**, and **LS-45**, respectively (Fig. 14), where the PCE increased in the order of **LS-43** (4.63%) < **LS-17** (5.16%) < **LS-45** (6.04%). The superior performance of **LS-45**, especially larger than that for **LS-11**, resulted from the larger J_{SC} and V_{OC} values, caused by the broadened and red-shifted absorption spectrum and larger CR resistance, respectively. Importantly, this general strategy can be a guideline for the further optimization of *meso*-substituted, air-stable bacteriochlorins.

6. Porphyrins created by unique synthetic strategies

6.1 Multi-fence porphyrins

As corroborated in bulky **YD2-*o*-C8**, the introduction of long alkoxy chains at *meso*-aryl substituents is an effective strategy to ensure a high blocking effect of CR between the redox couple and TiO_2 as well as to suppress the aggregation of porphyrins on TiO_2 because of the wrapping of the porphyrin core by multiple long alkoxy chains. Xie and co-workers[85] proposed a new class of doubly strapped porphyrin sensitizers, as represented by **XW40** and **XW41** (Fig. 15). In their synthetic scheme, 2,6-bis(octyloxy) phenyl groups at the *meso*-positions were replaced with 2,6-bis(hex-5-en-1-yloxy)phenyl groups (Scheme 19). The ring-closing metathesis reaction of precursor **86** with the 2nd generation Grubbs catalyst provided the doubly strapped porphyrin **87**, and then stepwise Sonogashira coupling reactions starting from **87** afforded **88** and the target molecule **89** with the push–pull structure. In contrast with the porphyrin **XW10** wrapped with four long alkoxyl chains (Fig. 15), **XW40** obtained a higher V_{OC} value (0.711 V *vs.* 0.730 V), because the introduction of the circle chain further inhibited the dye aggregation and CR. Additionally, a higher J_{SC} value (18.67 mA cm^{-2} *vs.* 17.90 mA cm^{-2}) was also attained because of the more compact structure of **XW40** and resulting increased dye-loading amount. Overall, **XW10** and **XW40** attained PCEs of 8.60% and 9.31%, respectively. Meanwhile, **XW41** with BTD as the auxiliary electron-withdrawing unit possessed a broader response spectral range than **XW40**, but the dye aggregation caused by the expansion of the π-conjugation led to a having a lower PCE of 8.16%. Enhanced efficiencies of 10.55% and 10.19% were obtained for **XW40**- and **XW41**-based DSSCs, respectively, through

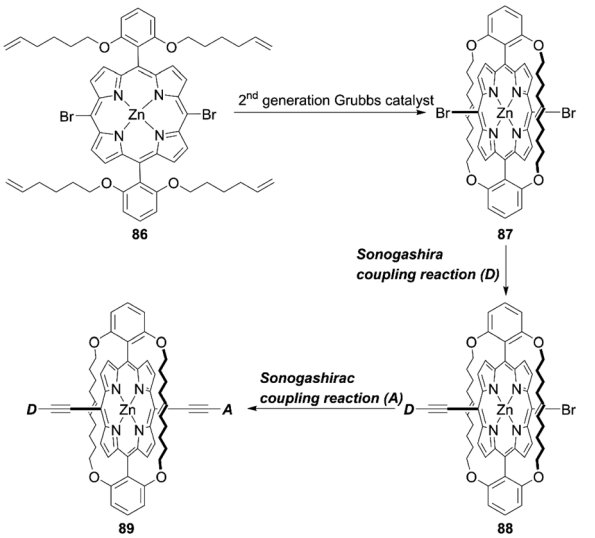

Scheme 19 Synthetic strategy for doubly strapped porphyrins.

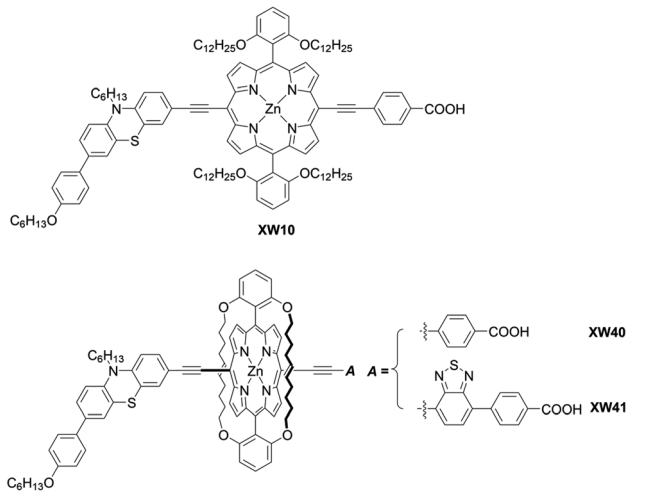

Fig. 15 Chemical structures of XW40, XW41, and XW10.

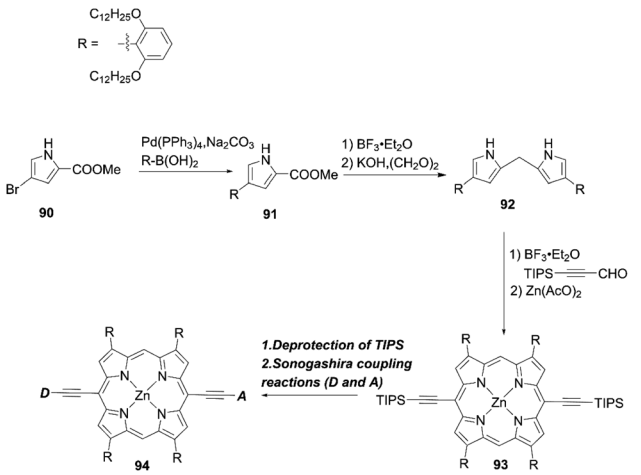

Scheme 20 Synthetic strategy for double-fence porphyrins.

a combined approach of co-adsorption (CDCA) and co-sensitization (**Z1**, Fig. 19).

Yeh and co-workers[86] put forward a new elegant approach to reduce dye aggregation and the CR process in which four β-phenyl rings were substituted with long alkoxyl groups at the β-positions of the porphyrin core. The key intermediate pyrrole **91** was prepared according to a Suzuki coupling reaction using the corresponding bromopyrrole **90** and boronic acid (Scheme 20). Then, subsequent condensation and decarboxylated reactions afforded the dipyrromethane **92**. Finally, the target molecule **94** was obtained by the acid-catalyzed condensation reaction of **92** with 3-(triisopropylsilyl)-1-propynal and the ensuing metalation, by the deprotection of **93** and a final Sonogashira coupling reaction.

The double-fence porphyrin sensitizers **bJS1–bJS3** (Fig. 16) achieved much higher PCEs (8.03–10.69%) than their single-fence analogues **mJS1–mJS3** (2.33–6.69%). Among the three double-fence porphyrins **bJS1–bJS3** in Fig. 16, the incorporation of benzotriazole and BTD units in the anchoring acceptor moiety for **bJS2** and **bJS3** caused further red-shifted absorption spectra, leading to high PCEs of 10.69% and 10.42%, respectively. These results exemplify that the introduction of multiple bulky substituents into the β-positions is an alternative fascinating strategy for the development of high-performance porphyrin-based DSSCs.

6.2 Porphyrins covalently linked to a co-sensitizer

Co-sensitization is widely used in DSSCs as an effective approach to improve the PCE. In general, two or more different dyes with complementary optical absorption characteristics are used to fully cover the solar spectrum, but generally it is

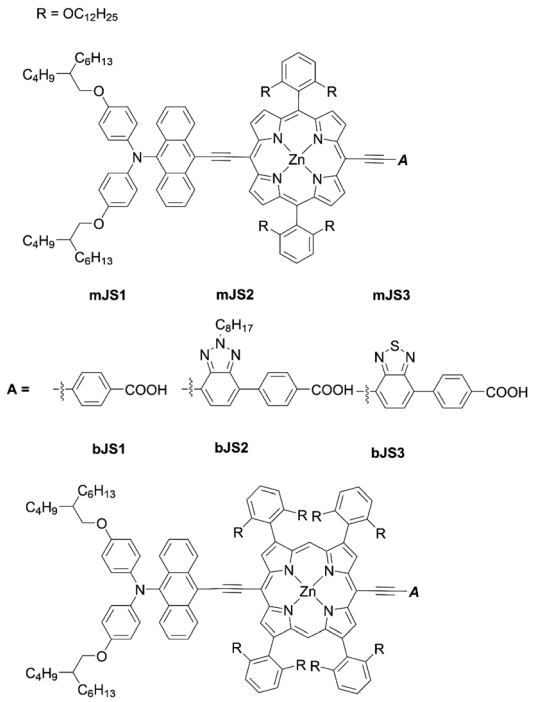

Fig. 16 Chemical structures of mJS1-3 and bJS1-3.

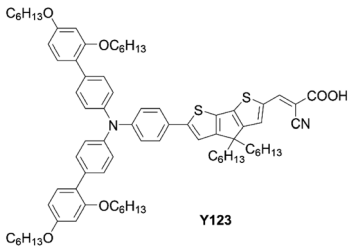

Fig. 17 Chemical structure of Y123.

necessary that the dyes have little intermolecular interactions on the TiO_2 surface. For example, the co-sensitization of **DfZnP-iPr+LEG4** and **YD2-*o*-C8+Y123** (Fig. 17), achieved higher PCEs than their single porphyrin systems without the addition of co-sensitizers as a consequence of their better light-harvesting abilities in the visible and near-infrared regions. However, traditional co-sensitization methods need many complicated optimization steps for attaining suitable adsorption conditions, while serious competitive adsorption frequently occurs between the main dye and the co-sensitizer.

Recently, Xie and co-workers[87] suggested an exotic approach for co-sensitization by designing "concerted companion dyes" (CC dyes), reporting **XW60-XW63** (Fig. 18). These dyes could be synthesized as shown in Scheme 21. Structurally, their difference was the length of the alkoxyl linker between the acceptor sides of **Z2** and **XW51** (Fig. 18). The key intermediate **96** was obtained by deprotection of the precursor **95** and a subsequent Sonogashira coupling reaction. Then, the further Suzuki coupling and hydrolysis reactions of **96** afforded the target molecule **97**. According to the DSSC obtained with the conventional co-sensitization method, where the TiO_2 film was immersed in the solution of **XW51** and **Z2** in sequence, the DSSC with **XW51+Z2** displayed a PCE of 9.2%. After optimizing

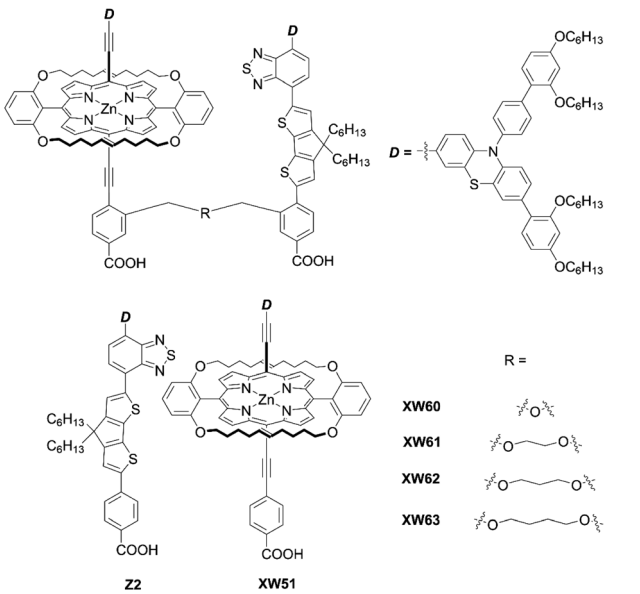

Fig. 18 Chemical structures of XW60-63, XW51, and Z2.

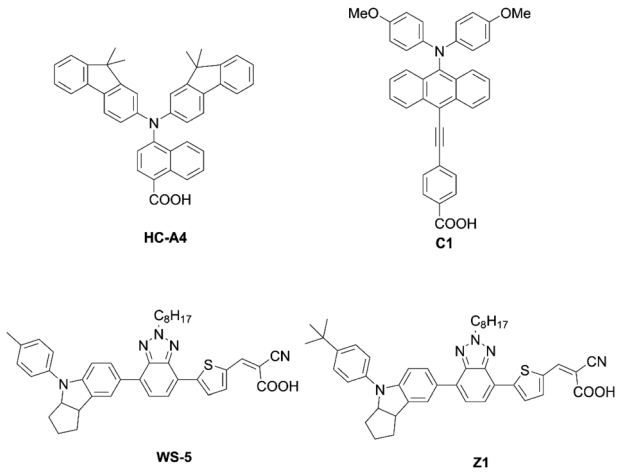

Fig. 19 Chemical structures of HC-A4, C1, WS-5, and Z1.

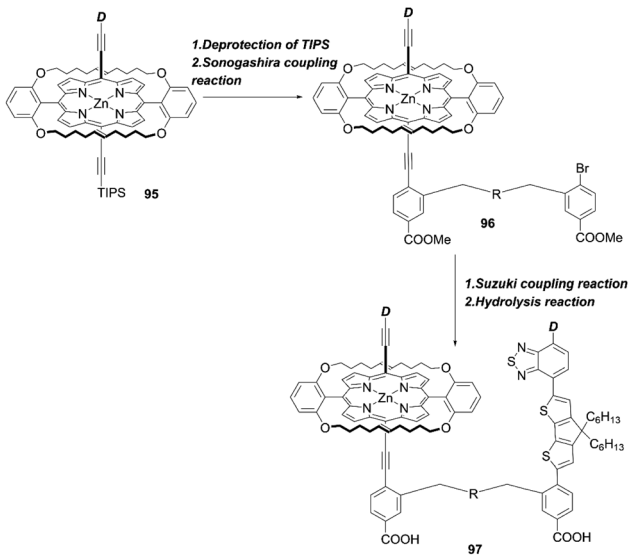

Scheme 21 Synthetic strategy for CC dyes. R = alkoxy linker.

the co-sensitization time and co-adsorption condition with CDCA, the PCE was slightly improved to 10.5%, but was still lower than the PCE of 11.1% obtained for the DSSC with **XW51**. This result may be explained by the drastic desorption of **XW51** dye from TiO_2 in the adsorption process of **Z2** onto TiO_2. Furthermore, during the co-sensitization process, some vacant sites generated by the desorption of **XW51** from TiO_2 would not be filled with **Z2** due to the mismatched spatial structure, leading to the occurrence of undesirable CR through the vacant hole on TiO_2. Interestingly, all the CC dyes except **XW60** exhibited enhanced PCEs of 11.6–11.7%. The reason for the decreased PCE obtained by the **XW60**-based DSSC may be due to the unfavourably tilted adsorption of the **Z2** component caused by the short bridging group.[47–49] On the other hand, the fact that nearly the same PCEs were achieved by the device with **XW61–63** indicated that the longer bridging group was unnecessary for highly efficient CC dyes. Furthermore, the co-adsorption of **XW61** with CDCA afforded a record PCE of 12.4% for iodine electrolyte-based DSSCs.

7. Summary and outlook

Many DSSCs have been developed hopefully as an alternative to silicon-based solar cells due to their ease of fabrication, cost-effectiveness, and environmental friendliness. Very recently, the highest PCE reported exceeded 15%.[89] Dyes play a crucial role in cell performance, and a lot of synthetic efforts have been paid to the development of new dyes showing high photovoltaic performance. In this context, porphyrins have drawn much attention because of their extraordinary high molar absorption coefficients of Soret and Q-bands around 400–600 nm. If the absorption is flattened at the wavelength of 400–800 nm, such porphyrins could be extremely promising in terms of their light-harvesting abilities. In this review article, we highlighted the synthetic strategies for preparing well-tailored porphyrins for DSSCs, aiming at a better light-harvesting property as well as reducing the aggregation on TiO_2 and increasing the blocking effect of the CR between TiO_2 and the electrolyte solution. It should be pointed out that it is still difficult to control the dye geometry on TiO_2, which affects the ET kinetics on TiO_2 and thereby the PCE, essentially because of the involvement of complicated multiple factors (*vide supra*). The following approaches have been taken for achieving a better light-harvesting property: (1) a push–pull D–π–A structure with suitable electron-donating and electron-withdrawing groups to strengthen ICT; (2) enlarging the π-conjugation, such as by fusion with peripheral aromatic rings; (3) lowering the symmetry of the porphyrins core by chemical modification. However, it should be noted here that elongation of the π-conjugation is always accompanied with serious dye aggregation, and sometimes leads to a more tilted geometry on the TiO_2 surface and a fast undesirable CR process. The introduction of bulky groups or alkyl/alkoxyl chains at the donor, porphyrin core, or acceptor is the general synthetic strategy to override these obstacles, but the try-and-error nature of experimentation is still a challenging process to optimize the properties. More importantly, the co-sensitization of dyes with complementary absorption is indispensable because even well-designed porphyrins have still a relatively weak light-harvesting property at 500–600 nm. Recently, copper(I/II) complexes have emerged as the third-generation redox couples[27,89,90] thanks to mitigation of the V_{OC} loss by the use of copper(I/II) complexes and by suppression of the nonradiative CR.[91] Generally, the first oxidation potential of most zinc porphyrin dyes usually lies at +0.8–1.0 V (*versus* NHE), which is similar to the redox potential of conventional copper redox shuttles. As a result of the mismatched energy levels, there is insufficient driving force for dye regeneration, which always leads to poor device performance. Accordingly, it is important to develop new porphyrins and copper redox shuttles that possess sufficient driving force for ET from the redox shuttle to the porphyrin radical cation (≥0.2 eV). Along this line, we achieved a PCE of 5.07% by selecting a suitable combination of an existing porphyrin and copper redox shuttle.[90] Shifting the redox potential of the copper redox

shuttles to a negative direction by adopting electron-donating ligands could be an option for a breakthrough. Besides, efficient synthetic strategies are needed to reduce the economic costs of dye synthesis towards large-scale commercial production. Although several novel reactions have been adopted to shorten the synthetic pathways (*i.e.* route b in Scheme 1), the number of required synthetic steps for obtaining high-performance porphyrins is still large (*i.e.* more than 10 steps for **SM315** from the commercial starting materials), which would lower the overall yield. Additionally, the use of noble metal catalysts (*i.e.* Pd-based complexes) should be optimized for further cost reduction.

It is noteworthy that, in recent years, machine learning (ML) has been developed rapidly. In this regard, there has been promising data-driven approaches reported for predicting the performance of new porphyrins[92] or organic dyes[93,94] to accelerate the discovery of potential sensitizers for DSSCs. Researchers have constructed a rational quantitative structure–property relationship (QSPR) model by ML based on reported dyes rather than first-principles equations, which can be used to predict the PCE of candidate dyes. ML-based approaches can greatly decrease the time, costs, and labour requirements compared to the common "trial and error" approach. Although the utility is still limited to the available reported data of sensitizers (10^2–10^3, which is much less than the widely preferred "big data"), we believe that it will become an effective tool for the design of dye sensitizers with high PCEs after further improvement.

Conflicts of interest

There are no conflicts to declare.

Acknowledgements

This work was supported by the JSPS (KAKENHI Grant Numbers JP20H05841 (T. H.) JP22K05066 (T. H.), JP20H05831 (H. I.), and JP20H05832 (H. I.)). Y. Zhang (CSC No. 202006250042) is grateful for the supports from the China Scholarship Council (CSC).

Notes and references

1 A. Hagfeldt, G. Boschloo, L.-C. Sun, L. Kloo and H. Pettersson, *Chem. Rev.*, 2010, **110**, 6595–6663.
2 B. O'Regan and M. Grätzel, *Nature*, 1991, **353**, 737–740.
3 M. K. Nazeeruddin, A. Kay, I. Rodicio, R. Humphry-Baker, E. Mueller, P. Liska, N. Vlachopoulos and M. Grätzel, *J. Am. Chem. Soc.*, 1993, **115**, 6382–6390.
4 M. K. Nazeeruddin, F. D. Angelis, S. Fantacci, A. Selloni, G. Viscardi, P. Liska, S. Ito, T. Bessho and M. Grätzel, *J. Am. Chem. Soc.*, 2005, **127**, 16835–16847.
5 M. K. Nazeeruddin, P. Péchy, T. Renouard, S. M. Zakeeruddin, R. Humphry-Baker, P. Comte, P. Liska, L. Cevey, E. Costa, V. Shklover, L. Spiccia, G. B. Deacon, C. A. Bignozzi and M. Grätzel, *J. Am. Chem. Soc.*, 2001, **123**, 1613–1624.
6 P. Wang, S. M. Zakeeruddin, P. Comte, R. Charvet, R. Humphry-Baker and M. Grätzel, *J. Phys. Chem. B*, 2003, **107**, 14336–14341.
7 C.-Y. Chen, M.-K. Wang, J.-Y. Li, N. Pootrakulchote, L. Alibabaei, C. Ngoc-le, J.-D. Decoppet, J.-H. Tsai, C. Grätzel, C.-G. Wu, S. M. Zakeeruddin and M. Grätzel, *ACS Nano*, 2009, **3**, 3103–3109.
8 Y.-Z. Wu, W.-H. Zhu, S. M. Zakeeruddin and M. Grätzel, *ACS Appl. Mater. Interfaces*, 2015, **7**, 9307–9318.
9 Z.-Y. Yao, H. Wu, Y.-M. Ren, Y.-C. Guo and P. Wang, *Energy Environ. Sci.*, 2015, **8**, 1438–1442.
10 Y. K. Eom, I. T. Choi, S. H. Kang, J. Lee, J. Kim, M. J. Ju and H. K. Kim, *Adv. Energy Mater.*, 2015, **5**, 1500300.
11 N. Koumura, Z.-S. Wang, S. Mori, M. Miyashita, E. Suzuki and K. Hara, *J. Am. Chem. Soc.*, 2006, **128**, 14256–14257.
12 Z.-Y. Yao, H. Wu, Y. Li, J.-T. Wang, J. Zhang, M. Zhang, Y.-C. Guo and P. Wang, *Energy Environ. Sci.*, 2015, **8**, 3192–3197.
13 Y. K. Eom, S. H. Kang, I. T. Choi, Y. Yoo, J. Kim and H. K. Kim, *J. Mater. Chem. A*, 2017, **5**, 2297–2308.
14 K. Kakiage, Y. Aoyama, T. Yano, T. Otsuka, T. Kyomen, M. Unno and M. Hanaya, *Chem. Commun.*, 2014, **50**, 6379–6381.
15 A. Kay and M. Grätzel, *J. Phys. Chem.*, 1993, **97**, 6272–6277.
16 T. Bessho, S. M. Zakeeruddin, C.-Y. Yeh, E. W.-G. Diau and M. Grätzel, *Angew. Chem., Int. Ed.*, 2010, **49**, 6646–6649.
17 A. Yella, H.-W. Lee, H. N. Tsao, C.-Y. Yi, A. K. Chandiran, M. K. Nazeeruddin, E. W.-G. Diau, C.-Y. Yeh, S. M. Zakeeruddin and M. Grätzel, *Science*, 2011, **334**, 629–634.
18 S. Mathew, A. Yella, P. Gao, R. Humphry-Baker, B. F. E. Curchod, N. Ashari-Astani, I. Tavernelli, U. Rothlisberger, M. K. Nazeeruddin and M. Grätzel, *Nat. Chem.*, 2014, **6**, 242–247.
19 A. Yella, C.-L. Mai, S. M. Zakeeruddin, S.-N. Chang, C.-H. Hsieh, C.-Y. Yeh and M. Grätzel, *Angew. Chem., Int. Ed.*, 2014, **53**, 2973–2977.
20 S. H. Kang, M. J. Jeong, Y. K. Eom, I. T. Choi, S. M. Kwon, Y. J. Yoo, J. H. Kim, J. Kwon, J. H. Park and H. K. Kim, *Adv. Energy Mater.*, 2017, **7**, 1602117.
21 H. Imahori, T. Umeyama and S. Ito, *Acc. Chem. Res.*, 2009, **42**, 1809–1818.
22 M. Urbani, M. Grätzel, M. K. Nazeeruddin and T. Torres, *Chem. Rev.*, 2014, **114**, 12330–12396.
23 H. Imahori, T. Umeyama, K. Kurotobi and Y. Takano, *Chem. Commun.*, 2012, **48**, 4032–4045.
24 T. Higashino and H. Imahori, *Dalton Trans.*, 2015, **44**, 448–463.
25 J.-M. Ji, H.-R. Zhou and H. K. Kim, *J. Mater. Chem. A*, 2018, **6**, 14518–14545.
26 K.-W. Zeng, Z.-F. Tong, L. Ma, W.-H. Zhu, W.-J. Wu and Y.-S. Xie, *Energy Environ. Sci.*, 2020, **13**, 1617–1657.
27 T. Higashino and H. Imahori, *ACS Energy Lett.*, 2022, **7**, 1926–1938.
28 C.-W. Lee, H.-P. Lu, C.-M. Lan, Y.-L. Huang, Y.-R. Liang, W.-N. Yen, Y.-C. Liu, Y.-S. Lin, E. W.-G. Diau and C.-Y. Yeh, *Chem. Eur. J.*, 2009, **15**, 1403–1412.

29 C.-M. Li, L. Luo, D. Wu, R.-Y. Jiang, J.-B. Lan, R.-L. Wang, L.-Y. Huang, S.-Y. Yang and J.-S. You, *J. Mater. Chem. A*, 2016, **4**, 11829–11834.
30 T. Higashino, Y. Fujimori, K. Sugiura, Y. Tsuji, S. Ito and H. Imahori, *Angew. Chem., Int. Ed.*, 2015, **54**, 9052–9056.
31 T. Higashino, Y. Kurumisawa, N. Cai, Y. Fujimori, Y. Tsuji, S. Nimura, D. M. Packwood, J. Park and H. Imahori, *ChemSusChem*, 2017, **10**, 3347–3351.
32 T. Higashino, S. Nimura, K. Sugiura, Y. Kurumisawa, Y. Tsuji and H. Imahori, *ACS Omega*, 2017, **2**, 6958–6967.
33 T. Higashino, H. Iiyama, Y. Kurumisawa and H. Imahori, *ChemPhysChem*, 2019, **20**, 2689–2695.
34 A. Hinsch, J. M. Kroon, R. Kern, I. Uhlendorf, J. Holzbock, A. Meyer and J. Ferber, *Prog. Photovolt: Res. Appl.*, 2001, **9**, 425–438.
35 R. B. Ambre, G.-F. Chang and C.-H. Hung, *Chem. Commun.*, 2014, **50**, 725–727.
36 L.-L. Li and E. W.-G. Diau, *Chem. Soc. Rev.*, 2013, **42**, 291–304.
37 D.-M. Shen, C. Liu, X.-G. Chen and Q.-Y. Chen, *J. Org. Chem.*, 2009, **74**, 206–211.
38 M. Yan, Q.-H. Wang, Y.-Z. Zhu, M.-L. Han, Y.-Q. Yan and J.-Y. Zheng, *J. Photochem. Photobiol. A*, 2021, **416**, 113325.
39 H.-H. Chou, K. S. K. Reddy, H.-P. Wu, B.-C. Guo, H.-W. Lee, E. W.-G. Diau, C.-P. Hsu and C.-Y. Yeh, *ACS Appl. Mater. Interfaces*, 2016, **8**, 3418–3427.
40 C.-F. Lo, S.-J. Hsu, C.-L. Wang, Y.-H. Cheng, H.-P. Lu, E. W.-G. Diau and C.-Y. Lin, *J. Phys. Chem. C*, 2010, **114**, 12018–12023.
41 Y.-Q. Wang, B. Chen, W.-J. Wu, X. Li, W.-H. Zhu, H. Tian and Y.-S. Xie, *Angew. Chem., Int. Ed.*, 2014, **53**, 10779–10783.
42 Y.-S. Xie, Y.-Y. Tang, W.-J. Wu, Y.-Q. Wang, J.-C. Liu, X. Li, H. Tian and W.-H. Zhu, *J. Am. Chem. Soc.*, 2015, **137**, 14055–14058.
43 Y.-Y. Tang, Y.-Q. Wang, X. Li, H. Ågren, W.-H. Zhu and Y.-S. Xie, *ACS Appl. Mater. Interfaces*, 2015, **7**, 27976–27985.
44 G.-S. Yang, Y.-Y. Tang, X. Li, H. Ågren and Y.-S. Xie, *ACS Appl. Mater. Interfaces*, 2017, **9**, 36875–36885.
45 H.-L. Song, J. Zhang, J.-M. Jin, H.-F. Wang and Y.-S. Xie, *J. Mater. Chem. C*, 2018, **6**, 3927–3936.
46 C.-L. Wang, C.-M. Lan, S.-H. Hong, Y.-F. Wang, T.-Y. Pan, C.-W. Chang, H.-H. Kuo, M.-Y. Kuo, E. W.-G. Diau and C.-Y. Lin, *Energy Environ. Sci.*, 2012, **5**, 6933–6940.
47 H. Imahori, S. Kang, H. Hayashi, M. Haruta, H. Kurata, S. Isoda, S. E. Canton, Y. Infahsaeng, A. Kathiravan, T. Pascher, P. Chábera, A. P. Yartsev and V. Sundström, *J. Phys. Chem. A*, 2011, **115**, 3679–3690.
48 S. Ye, A. Kathiravan, H. Hayashi, Y. Tong, Y. Infahsaeng, P. Chabera, T. Pascher, A. P. Yartsev, S. Isoda, H. Imahori and V. Sundström, *J. Phys. Chem. C*, 2013, **117**, 6066–6080.
49 H. Imahori, *Bull. Chem. Soc. Jpn.*, 2023, DOI: **10.1246/bcsj.20230031**.
50 T. Higashino, Y. Kurumisawa, S. Nimura, H. Iiyama and H. Imahori, *Eur. J. Org. Chem.*, 2018, 2537–2547.
51 K. Kurotobi, Y. Toude, K. Kawamoto, Y. Fujimori, S. Ito, P. Chabera, V. Sundström and H. Imahori, *Chem. Eur. J.*, 2013, **19**, 17075–17081.
52 T. Higashino, K. Kawamoto, K. Sugiura, Y. Fujimori, Y. Tsuji, K. Kurotobi, S. Ito and H. Imahori, *ACS Appl. Mater. Interfaces*, 2016, **8**, 15379–15390.
53 G. D. Carlo, A. O. Biroli, M. Pizzotti, F. Tessore, V. Trifiletti, R. Ruffo, A. Abbotto, A. Amat, F. D. Angelis and P. R. Mussini, *Chem. Eur. J.*, 2013, **19**, 10723–10740.
54 K. Sudhir, K. S. K. Reddy, Y.-C. Liu, H.-H. Chou, K. Kala, T.-C. Wei and C.-Y. Yeh, *ACS Appl. Mater. Interfaces*, 2018, **10**, 39970–39982.
55 H. Hata, H. Shinokubo and A. Osuka, *J. Am. Chem. Soc.*, 2005, **127**, 8264–8265.
56 The names of the dyes were previously given as **tda-1b-d-Zn** and **tda-2b-bd-Zn**, respectively. See: M. Ishida, S. W. Park, D. Hwang, Y. B. Koo, J. L. Sessler, D. Y. Kim and D. Kim, *J. Phys. Chem. C*, 2011, **115**, 19343–19354.
57 M. Ishida, D. Hwang, Y. B. Koo, J. Sung, D. Y. Kim, J. L. Sessler and D. Kim, *Chem. Commun.*, 2013, **49**, 9164–9166.
58 M. Ishida, D. Hwang, Z. Zhang, Y. J. Choi, J. Oh, V. M. Lynch, D. Y. Kim, J. L. Sessler and D. Kim, *ChemSusChem*, 2015, **8**, 2967–2977.
59 M. Tanaka, S. Hayashi, S. Eu, T. Umeyama, Y. Matano and H. Imahori, *Chem. Commun.*, 2007, 2069–2071.
60 S. Hayashi, M. Tanaka, H. Hayashi, S. Eu, T. Umeyama, Y. Matano, Y. Araki and H. Imahori, *J. Phys. Chem. C*, 2008, **112**, 15576–15585.
61 S. Eu, S. Hayashi, T. Urneyama, Y. Matano, Y. Araki and H. Imahori, *J. Phys. Chem. C*, 2008, **112**, 4396–4405.
62 H. Hayashi, A. S. Touchy, Y. Kinjo, K. Kurotobi, Y. Toude, S. Ito, H. Saarenpää, N. V. Tkachenko, H. Lemmetyinen and H. Imahori, *ChemSusChem*, 2013, **6**, 508–517.
63 S. Hayashi, Y. Matsubara, S. Eu, H. Hayashi, T. Umeyama, Y. Matano and H. Imahori, *Chem. Lett.*, 2008, **37**, 846–847.
64 R. Deshpande, L. Jiang, G. Schmidt, J. Rakovan, X.-P. Wang, K. Wheeler and H. Wang, *Org. Lett.*, 2009, **11**, 4251–4253.
65 Y. Hu, W. A. Webre, M. B. Thomas, A. Moss, S. N. Hancock, J. Schaffner, F. D'Souza and H. Wang, *J. Mater. Chem. A*, 2019, **7**, 10712–10722.
66 Y. Hu, A. Alsaleh, O. Trinh, F. D'Souza and H. Wang, *J. Mater. Chem. A*, 2021, **9**, 27692–27700.
67 J. Luo, M.-F. Xu, R.-Z. Li, K.-W. Huang, C.-Y. Jiang, Q.-B. Qi, W.-D. Zeng, J. Zhang, C.-Y. Chi, P. Wang and J.-S. Wu, *J. Am. Chem. Soc.*, 2014, **136**, 265–272.
68 Y. Kurumisawa, T. Higashino, S. Nimura, Y. Tsuji, H. Iiyama and H. Imahori, *J. Am. Chem. Soc.*, 2019, **141**, 9910–9919.
69 J. T. Dy, K. Tamaki, Y. Sanehira, J. Nakazaki, S. Uchida, T. Kubo and H. Segawa, *Electrochemistry*, 2009, **77**, 206–209.
70 A. J. Mozer, M. J. Griffith, G. Tsekouras, P. Wagner, G. G. Wallace, S. Mori, K. Sunahara, M. Miyashita, J. C. Earles, K. C. Gordon, L. Du, R. Katoh, A. Furube and D. L. Officer, *J. Am. Chem. Soc.*, 2009, **131**, 15621–15623.
71 J.-W. Shiu, Y.-C. Chang, C.-Y. Chan, H.-P. Wu, H.-Y. Hsu, C.-L. Wang, C.-Y. Lin and E. W.-G. Diau, *J. Mater. Chem. A*, 2015, **3**, 1417–1420.
72 T. Higashino, K. Sugiura, Y. Tsuji, S. Nimura, S. Ito and H. Imahori, *Chem. Lett.*, 2016, **45**, 1126–1128.

73 T. Zhang, X. Qian, P.-F. Zhang, Y.-Z. Zhu and J.-Y. Zheng, *Chem. Commun.*, 2015, **51**, 3782–3785.
74 A. Osuka and H. Shimidzu, *Angew. Chem., Int. Ed. Engl.*, 1997, **36**, 135–137; *Angew. Chem.*, 1997, **109**, 93–95.
75 N. Yoshida, H. Shimidzu and A. Osuka, *Chem. Lett.*, 1998, **27**, 55–56.
76 L.-M. Jin, L. Chen, J.-J. Yin, C.-C. Guo and Q.-Y. Chen, *Eur. J. Org. Chem.*, 2005, 3994–4001.
77 T. Higashino, Y. Kurumisawa, H. Iiyama and H. Imahori, *Chem. Eur. J.*, 2019, **25**, 538–547.
78 X.-F. Wang, H. Tamiaki, L. Wang, N. Tamai, O. Kitao, H. Zhou and S. Sasaki, *Langmuir*, 2010, **26**, 6320–6327.
79 X.-F. Wang, O. Kitao, H. Zhou, H. Tamiaki and S. Sasaki, *J. Phys. Chem. C*, 2009, **113**, 7954–7961.
80 X.-J. Liu, C.-J. Li, X. Peng, Y.-Z. Zhou, Z. Zeng, Y.-C. Li, T.-Y. Zhang, B. Zhang, Y. Dong, D.-M. Sun, P. Cheng and Y.-Q. Feng, *Dyes Pigm.*, 2013, **98**, 181–189.
81 T. Higashino, Y. Tsuji, Y. Fujimori, K. Sugiura, S. Ito and H. Imahori, *Chem. Lett.*, 2015, **44**, 1395–1397.
82 S. Chakraborty, H.-C. You, C.-K. Huang, B.-Z. Lin, C.-L. Wang, M.-C. Tsai, C.-L. Liu and C.-Y. Lin, *J. Phys. Chem. C*, 2017, **121**, 7081–7087.
83 H.-J. Kim and J. S. Lindsey, *J. Org. Chem.*, 2005, **70**, 5475–5486.
84 S. Chakraborty, M.-C. Tsai, X.-D. Su, X.-C. Chen, T.-T. Su, C.-K. Tsao and C.-Y. Lin, *RSC Adv.*, 2020, **10**, 6172–6178.
85 K.-W. Zeng, Y.-Y. Lu, W.-Q. Tang, S.-L. Zhao, Q.-Y. Liu, W.-H. Zhu, H. Tian and Y.-S. Xie, *Chem. Sci.*, 2019, **10**, 2186–2192.
86 C.-C. Chen, J.-S. Chen, V. S. Nguyen, T.-C. Wei and C.-Y. Yeh, *Angew. Chem., Int. Ed.*, 2021, **60**, 4886–4893.
87 K.-W. Zeng, Y. Chen, W.-H. Zhu, H. Tian and Y.-S. Xie, *J. Am. Chem. Soc.*, 2020, **142**, 5154–5161.
88 K.-W. Zeng, W.-Q. Tang, C.-J. Li, Y.-Y. Chen, S.-L. Zhao, Q.-Y. Liu and Y.-S. Xie, *J. Mater. Chem. A*, 2019, **7**, 20854–20860.
89 Y. Ren, D. Zhang, J. Suo, Y. Cao, F. T. Eickemeyer, N. Vlachopoulos, S. M. Zakeeruddin, A. Hagfeldt and M. Grätzel, *Nature*, 2023, **613**, 60–65.
90 T. Higashino, H. Iiyama, I. Nishimura and H. Imahori, *Chem. Lett.*, 2020, **49**, 936–939.
91 H. Imahori, Y. Kobori and H. Kaji, *Acc. Mater. Res.*, 2021, **2**, 501–514.
92 C.-C. Fan, M. Springborg and Y.-Q. Feng, *Phys. Chem. Chem. Phys.*, 2019, **21**, 5834–5844.
93 H. Li, Z. Zhong, L. Li, R. Gao, J. Cui, T. Gao, L. H. Hu, Y. Lu, Z.-M. Su and H. Li, *J. Comput. Chem.*, 2015, **36**, 1036–1046.
94 Y.-P. Wen, L.-L. Fu, G.-Q. Li, J. Ma and H.-B. Ma, *Sol. RRL*, 2020, **4**, 2000110.